Experimental study on steel-reinforced concrete-filled steel tubular columns under the fire

Wen-Jing Mao[a], Wen-Da Wang[a,*], Kan Zhou[b], Er-Feng Du[c]

[a] *School of Civil Engineering, Lanzhou University of Technology, Lanzhou 730050, P.R. China*

b Faculty of Engineering and Informatics, University of Bradford, Bradford, West Yorkshire, BD7 1DP, United Kingdom

[c] *School of Civil Engineering, Southeast University, Nanjing 211189, P.R. China*

Abstract: This paper aims to experimentally study the fire performance of steel-reinforced concrete-filled steel tubular (SRCFST) columns without fire protection. Eight SRCFST specimens with cruciform section profiled steel were tested under the ISO-834 standard fire. The various test parameters including cross-section type of steel tube (circular or square), the load ratio and load eccentricity were considered and discussed. The temperature distribution, failure modes, axial and lateral deformation, fire resistance of the specimens obtained by test were investigated in detail. The results show that the cruciform section profiled steel provided great confinement effect to core concrete, and can efficiently suppress the generation and development of cracks in concrete. The specimens with diverse load ratio or loading method present various tendency of axial deformation versus time curves, i.e. five stages for axially loading specimens with common load ratio (n=0.4) and three stages for specimens with high load ratio (n>0.4) or specimens under eccentric compression. The critical temperature of SRCFST specimens is much lower than that of steel structures and CFST columns at same parameters, and the fire resistance of SRCFST columns has significant improvement compared with CFST columns. Moreover, available design method for SRCFST columns and CFST columns were compared with test results to evaluate the applicability for SRCFST specimens.

Keywords: steel-reinforced concrete filled steel tubular (SRCFST) columns; failure mode; critical temperature; fire resistance

*Corresponding author. Tel./fax: +86 931 2350533;

Wen-Da Wang, Professor of School of Civil Engineering, Lanzhou University of Technology, China

E-mail: wangwd@lut.edu.cn (W.-D. Wang).

1. Introduction

With the continuous development of high-rise, large-span and heavy-loading buildings, some innovative material and forms of cross-section have been proposed and developed to deal with the progressively developed demands for modern structure[1-2]. Branching from conventional concrete filled steel tubular (CFST) columns, steel-reinforced concrete-filled steel tubular (SRCFST) members, comprising hollow steel tube, concrete and inserted profiled steel, was proposed in EN 1994-1-1 [3] firstly.

This composite columns are commonly used in current research and engineering serving as vertical load bearing members, to achieve a distinctly enhanced bearing capacity. Fig.1 shows typical cross-section of SRCFST members. The sectional dimension of SRCFST columns can be reduced compared with CFST columns for a given load, the restraint of profiled steel enhanced the strength and ductility of the concrete[4]. The beneficial effects of profiled steel can surely improve structural behaviour [5, 6], thus SRCFST columns are suitable to meet the fire-resistance requirement in heavy-loading building.

The existing extensive literature on mechanical properties of SRCFST structures at ambient temperature, including static and dynamic behaviour, confirms the superiority of structural behaviour. Wang *et al.* [4] and Zhu *et al.* [6] examined the mechanical behaviour of SRCFST columns, including stub and long columns under axial load via combine of test and numerical analysis. The experimental and numerical investigations were performed on axially loaded SRCFST stub columns by Ding *et al.* [5]. Chang *et al.* [7] and Farajpourbonab *et al.* [8] numerically analysed the mechanical behaviour of SRCFST columns subjected to cyclically loaded based on FEA model. Shi *et al.* [9, 10] conducted the mechanical experiments of circular SRCFST member under lateral shear load and pure bending loads. Xian *et al.* [11] carried out the experiment on dynamic response of circular SRCFST members under lateral impact loads.

Wang *et al.* [12, 13] investigated the flexural performance of SRCFST members and behaviour of SRCFST members under combined compression and torsion. The researches above provide important insights to mechanical behaviour of SRCFST columns. Three components, i.e. steel tube, concrete and profiled steel are combined in a particular way, which inherit the advantages of CFST members such as high bearing capacity, good ductility, and superior seismic.

In additional, similar to CFST columns [14-19], preliminary study showed that embedded profiled steel has great contributions to the fire resistance of SRCFST structures. Espinos *et al.* [20] conducted a numerical investigation on method of improving the fire performance of CFST columns by insert profiled steel, including circular steel tube, steel core and H-shaped steel. Tan *et al.* [21] carried out a FE analysis for concrete-filled stainless steel tubular (CFSST) columns and steel-reinforced CFSST on fire behaviour. Zhu *et al.* [22] and Meng *et al.* [23] performed experimental investigation on the fire resistance of SRCFST columns subjected to uniform and non-uniform fire conditions and residual strength of square SRCFST columns after exposure fire. Besides, the fire performance of concrete-filled steel tube columns with solid steel core was investigated by Neuenschwander [24, 25] *et al.*, Klingsch [26], Schaumann and Kleibömer [27] investigated the fire performance. The preliminary study indicated that for CFST columns with embedded profiled steel or steel core, heating rate and fire resistance have significant improvement. For SRCFST members, the embedded profiled steel is advantageous to load-carrying capacity and ductility of composite members at elevated temperature, and it is the major factor of delaying and restraining inclined cracks in concrete. And simultaneously, the insulation function of concrete can serve as a fire protection for profiled steel.

However, the limit experimental data and systematic understanding is available on fire performance of SRCFST columns, the existing parameters and variety of experimental specimens are limited because

of the test facility limits and cost, although this kind of composite columns is applied in building practice. It is necessary for further understanding the structural fire performance of SRCFST columns from database. Meanwhile, the test data is not enough to validate the accurate the modelling approach although the finite element analysis has been used to investigate the fire resistance performance of SRCFST columns, there is room for expansion of experimental data. Additional, taking into account beneficial effect of profiled steel, it is essential to assess the accuracy of the current design method for fire resistance of composite columns. In view of scarcity of researches on SRCFST columns, fire test of SRCFST columns can prove sufficient test data for a new and improved design method in follow-up study.

Based on the previous researches and results, an experimental study is conducted on the temperature field and fire resistance of eight SRCFST columns to explore the mechanical performance of SRCFST columns under the fire. The test parameters, including cross-section type of steel tube (circular or square), the load ratio, load eccentricity were considered. The heat transfer mechanism at elevated temperature, deformation versus time relationship, failure models, critical temperature of steel tube and fire resistance were analysed in detail. Additional, the measured fire resistance of specimens were predicted according to formulations for CFST columns and simple calculation model in EN 1994-1-2 to verify the applicability.

2. Experimental procedure

2.1 Specimen preparation

Eight specimens was designed to the Chinese codes GB 50936-2014 [28], JGJ138-2016 [29] and YB 9082-2006[30]. The capacity of the test loading device and specifications of the thin-wall straight seam welded tube were also taken into account. Test parameters were the cross-section shape of the steel tube (4 of circular cross-section and 4 of square cross-section), load ratio and load eccentricity. The load ratio, n, is defined as $n=N_F/N_u$, where N_F is the load applied to the columns in test, and N_u is the resistance of

the column in axial compression at ambient temperature which can be calculated based on EN 1994-1-1:2004 [3]. Four specimens feature a circular section of 325mm in diameters and wall thickness of 6mm, and other specimens with a square cross-section of 300mm and a wall thickness of 5.5mm were used. All specimens featured a cruciform steel section embedded in concrete. The dimensions ($h \times b \times d \times t_w$) of cruciform section profiled steel embedded in circular and square cross-section were 140mm×70mm×5mm×8mm and 160mm×90mm×5mm×8mm, respectively, where h, b, d and t_w are the web height, the flange width, the web thickness and the flange thickness, respectively. The profiled steels were classified as A or B for circular and square cross-section, respectively. The specimen labels and detailed parameters are summarised in Table 1. It was labelled in such a manner of CSU-Z-40 for SRCFST members. In the specimen labels, ‘CS’ and ‘SS’ indicated the cross-section type in the first phrase, i.e. circular and square SRCFST column. ‘U’ denotes the uniform fire exposure. ‘Z’ represents concentric loading. ‘P50’ and ‘P80’ denote eccentricity of loading of 50mm and 80mm, respectively. The last two digits denotes the load ratio, e.g., ‘40’ means the load ratio is 0.40. Note that the actual load applied during test were slightly deviated from the designed values, due to large tonnage of the jack required in fire test and operational error.

The steel tube was straight seam welded tubes. To facilitate the loading at the top end and its connection with the hinged support, end plates with a thickness of 30mm were welded to the top and bottom ends. Additionally, a hole with same size as profiled steel was cut in centre of the top end plate. The steel tubes for all specimens were each cut to length, and simultaneously the length of profiled steel needed to exceed 30mm (the thickness of end plate) than length of steel tube. Additionally, the holes, served as thermocouples measured for temperature in concrete, in steel tube with a diameter of 40mm were prepared. The profiled steel was welded centrically to the bottom end plate, and stirrups served as

fixation for thermocouples were fixed onto the profiled steel in a first assembly step. Fig. 2 presents the details of the specimens. After mounting all thermocouples measured for temperature in profiled steel against the stirrups, the steel tube was assembled carefully with profiled steel and bundles of thermocouples, which were run through the holes of steel tube at the bottom of columns. Then the steel tube was welded against the bottom end plate, which was kept concentrically with respect to the profiled steel. After casting concrete into the hollow columns, the top end plate with a hole was inserted into profiled steel and fixed with the steel tube and profiled steel by fillet welding, and the steel sheets with a diameter of 40mm were welded for repairing the holes in steel tube finally.

For the axial loaded specimens (Fig.2d), their centroid of the steel section coincided with that of the end plate. For specimens loaded with an eccentricity of 50 mm, the centroid of the specimens also coincide with that of the end plate; but the positions of the screw hole were adjusted so that the eccentricity can be introduced by means of the distance between the end plate centre and the bearing centre. For specimens loaded with an eccentricity of 80 mm, the positions of the screw holes was kept the same with Fig.2e. To introduce the additional 30 mm eccentricity, the specimen centroid was moved 30 mm away from the centroid of the end plate. In addition, stiffeners (Fig.2a) were used at the ends of the column to enhance the rigidity.

2.2 Material properties

The mechanical properties of steel at ambient temperature were determined by standard tensile tests. Taking the slats from the reserved steel, including circular or square steel tube, welded profiled steel, the tensile standard parts were prepared, three for each type of steel. The steel of the corner of the square steel tube were cut and stretched within the valid width to completely evaluate the tensile strength of square steel tube. Tensile tests were conducted according to the method specified, and the average yield strength

(f_y), the ultimate tensile strength (f_u), the elastic modulus (E_s), Poisson's ratio (μ) and the elongation (δ_{10}) were measured. An error analysis was performed of each group of test data to obtain the average values used in this test, as summarised in Table 2.

For the concrete infill, commercial concrete of grade C50 containing 42.5# ordinary Portland cement, fine aggregates (fineness modulus of 2.9), limestone gravel (5-20mm) and filler was used. The mix proportion was: water, 148kg/m^3, cement, 425kg/m^3, pulverized coal ash, 65kg/m^3, mineral powder, 48kg/m^3, fine aggregate, 718kg/m^3, coarse aggregate, 1014kg/m^3 and water reducing agent, 9.2kg/m^3. The cube compressive strength of three concrete cubes of 150×150×150 mm in dimensions were tested, and the average cube compressive strength of concrete at 28 days and the time of test (125 days) was 47.4MPa and 64.4MPa, respectively.

2.3 Test setup and boundary conditions

The fire resistance tests were carried out in the vertical structural components furnace in Southeast University, China (Fig. 3). The testing equipment consists of a furnace, a pressure control panel, a load cell, a reaction frame, a data acquisition system and a hydraulic station system.

The furnace chamber with an internal dimensions of 3×3×3 m is divided into a fixed half and a demountable half. The central 3 m of the specimens was exposed to fire during the tests. The loading device at the top and the boundary at the bottom were wrapped with ceramic fibre blanket. During the tests, the furnace temperature was controlled by 16 burners and measured by 25 thermocouples mounted in the furnace. The test furnace meets the technical specifications and requirements for fire test of column components stipulated in ISO-834 [31].

The pined end condition was achieved by using the rollers at the top and the bottom ends (Fig. 4). Rotation was allowed in one direction, i.e., the direction perpendicular to the photo (Fig. 4a). The lateral

restraints were provided by additional device that was connected to the reaction frame (Fig.4b). Vertical movement of the top end was allowed. This was realised by restraining the movement of the wheels that were connected to the top end plate. These wheels were moving in a track that was fixed with the reaction frame system.

2.4 Measurement

A total of 25 thermocouples were installed at different heights inside the furnace to measure the furnace temperature. The specimen temperature were measured using the thermocouple embedded in the specimens. The positions of the measuring tips of these thermocouples are shown in Fig. 5. To highlight any difference in temperature along the longitudinal direction, thermocouples of the same layout were mounted within two cross-sections, which were the mid-height cross-section and the cross-section of 1 m lower. The numbers in the parentheses denote the labels of the thermocouples at the lower cross-section. For measurement points 1(5), 2(7), 3(8) and 4(9), the measuring tips of the thermocouples were adhered to the profiled steel. Measurement points 5(10) were located at 1/4 of diagonal of concrete section, as shown in Fig. 5. The surface temperature of steel tube were measured via measurement points 11(12).

Two displacement gauges placed on the upper end plate of the top hinge were used to measure the axial deformation and lateral deformation of test specimens. For convenient measurement of the lateral deformation, a stainless steel wire with maximum operating temperature of 1250 ℃ and diameter of 1.2 mm was fixed at the mid-height, and simultaneously it was led from the furnace to the outside to connect with a displacement gauge at the same height outside the furnace. The coefficient of linear expansion of resistance wire α_c was taken as 1.6×10^{-5}/℃(200℃-1000℃). Therefore, the expansion deformation caused by resistance wire (up to 21.4mm) during the fire test have been eliminated completely for actual results.

2.5 Test conditions and procedures

During the tests, after the column was installed into the fire furnace, the end plates of specimens were connected to the plates of the bearing using high-strength bolts. The thermocouples and the displacement sensors were wired to connect with data acquisition system firstly, and pre-load of 200 to 260 kN was subsequently applied to close the gaps between the end plates and the bearing. This pre-load was held for 10 min to check the data acquisition system. The test procedures consisted two phases as follows:

(1) Loading at ambient temperature. The load (Table 1) was applied incrementally (in 10 steps) and held for at least two minutes at each step until the displacement readings were steady. The axial deformation and lateral deformation were recorded.

(2) Testing of specimens in the standard fire. All test specimens were subjected to the uniform fire exposure. The furnace temperature was controlled to follow the ISO-834 [31] standards curve. The test furnace was controlled manually at the initial stage of fire exposure. When the furnace temperature rose to 200 °C at approximately 4 min, the control was switched to the automatic mode. Meanwhile, the temperature, axial deformation and lateral deformation were recorded. The load applied on the SRCFST specimens was kept constant by adjusting the loading jack during the fire exposure. When the bearing capacity of SRCFST specimens dropped dramatically and to maintain the load level the hydraulic stabilizer continuously controlled the pressure, the specimens were about to reach the fire resistance and the failure of SRCFST columns occurred finally

The criteria for failure in ISO-834 [31] was used for the tests: (1) the limiting rate of axial contraction reaches 0.003H (mm/min); (2) the limiting axial contraction reaches 0.01H (H stands for the initial height, unit in mm). For the specimens herein, the limiting axial contraction was 42.1 mm and the

limiting rate of axial contraction was 12.63 mm/min.

3. Experimental results and analysis

The experimental results and analyses of SRCFST specimens subjected to fire exposure, which can be divided into three subsection, are presented in this section. In the first subsection, the posttest examination consisted of failure modes, the opening of the steel tube and outer concrete are outlined. The temperature histories in all measurement point of cross-section during the fire are discussed in the second subsection, t. In the third subsection, the results of axial and lateral displacement recordings of the tested specimens are outlined and the development tendency of deformation under different load ratio are discussed.

3.1 Test observation and failure modes

3.1.1 Global failure modes

During the heating process, it is observed that water vapour started to escape from the top of the furnace when the average furnace temperature reached around 300 °C, and water vapour became obvious at 500°C. The specimen began to make intermittent sounds after 10 minutes of heating when the average furnace temperature was around 650 °C.

To further investigate the mechanical properties of SRCFST columns after fire test, all specimens were examined in detail. The comparisons of global failure modes for all SRCFST specimens are presented in Fig.6. Note that Fig.6 shows the residual deformation of the SRCFST columns after unloading; the actual deformation during fire exposure could be greater. The SRCFST specimens exhibited global buckling failure modes. All specimens proved a visible lateral deflection, and the location of the peak value of lateral bending for all specimens situated slightly above the mid-span of column. For specimens CSU-Z-50, CSU-P80-40, SSU-Z-50 and SSU-P80-40, the maximum lateral

deflection occurred at 620, 394, 370 and 260 mm above the mid-height, respectively.

Several reasons may account for phenomenon mentioned above: (1) discrepancy of boundary conditions between the top and bottom roller bearing. The bottom roller bearing was fixed with concrete pier on the ground by high-strength bolts. A gap of 1-2mm between pulleys welded on both sides of the top bearing and track of later restraint device might be reserved to install specimens, although the lateral deformation of top bearing was restrained, as illuminated in subsection 2.3. In addition, the gaps of both sides of top bearing were not identical caused by deviations of fabrication and installation. Thus, the restraint effect of top bearing was less to specimens compared with the bottom bearing; (2) the frictional effects for the roller bearing at the bottom maybe have been greater than at the top because of above mentioned; and (3) incompletely symmetrical end conditions has greater impacts for specimens CSU-Z-50, CSU-P80-40, SSU-Z-50 and SSU-P80-40 because of larger fire load level of them.

Evident local buckling of steel tube were observed. For SRCFST members of circular cross-section, the steel tubes exhibited local swelling along the radial direction, and it was more obvious on the compression side. For SRCFST members of square cross-section, the compression face and its two adjacent faces displayed obvious undulating buckling. This it more distinct for SRCFST specimens under the axial compression, because the second-order effect for the specimens subjected to eccentric compression is more pronounced, resulting in greater lateral deformation and faster instability.

For specimens of circular cross-section, for example, CSU-P50-40, local buckling near the position for the inner thermocouples was observed on the compression side of the steel tube (Fig. 7(a)), and a part of welds were torn. This is possible because: (1) the welding residual stress was unavoidable; and (2) an aperture of 8mm in diameters at the centre of steel sheet, to embed thermocouple of concrete, had weakening for cross-section under axial load. Therefore, the steel tube around welding occurred obvious

local buckling.

As presented in Fig. 7(b), for specimens of square cross-section, taking specimen SSU-P50-40 as an example, the steel tube on the compression side ruptured along the circumferential direction. The concrete infill was crushed, as shown in Fig. 7(c), and mortars were observed in all the vent holes of the specimen after test.

The apparent colour of cooled steel tube varies depending on varying heating time, and gradually deepens as the increase of the maximum temperature during the fire [32]. Details about apparent characteristics of steel tube under the fire are summarised in Table 3. When the maximum temperature of steel tube was around 400°C, the surface of steel tube was dark red; the steel pipe was taupe and tarnish at 500°C; When the surface temperature exceeded 600°C, the steel tube was black, and the oxide layers was partially swollen and falling off (Fig. 7(d)). The apparent features of steel tube observed by test were almost identical to summary available in [32], nevertheless the surface colour has difference at the maximum temperature of around 400°C because of several discrepancies for steel tube, such as steel types, cooling mode, the degree of corrosion and smoothness.

3.1.2 Inner failure state

To analyse the failure state of inner section clearly, the concrete is divided in detail, as shown in Fig. 2(b-c). In order to further examine and analyse the inner failure state of SRCFST members under the fire, the outer steel tube was cut open and removed for a clearer view of concrete and profiled steel. For SRCFST columns of circular cross-section, it is difficult to remove the steel tube. By comparison, for square SRCFST specimens, separation in the interface of steel tube and outer concrete at the compression region was observed. In addition, the steel plate fell off immediately when the corner of square steel tube was cut longitudinally. The difference could be attributed to the difference of confinement effect; the

confinement effect for the circular cross-section is more uniformed distributed than that for the square cross-section according to previous research of CFST members [33]. For square steel tube, the confinement stress is minimized at the midpoint of the edges, whilst peaks at the corner zone. This forms a weak constraint area, as illustrated in Fig. 8. In addition, the midpoint of the edges of whole square cross-section had the least confinement force, followed by the centre of the cross section. Thus, the confinement effect of square steel tube on concrete had significant reduction compared with that of circular steel tube (around 70%) [34].

Typical failure modes of concrete are presented in Fig.9 and Fig. 10, taking specimens CSU-Z-40 and SSU-Z-40 as example. No major crushing was observed for the concrete as a result of the confinement of the steel tube. As presented in Fig. 9(b), few crushed concrete appeared on the concrete surface of specimen CSU-Z-40, while the concrete at the pressure side of specimen SSU-Z-40 and two adjacent sides had obvious crushing, chipping and shedding in the mid-column area, as presented in Fig. 10(b). For specimen CSU-Z-40, a transverse crack of 2 to 5mm in width was observed on the tension side, which was caused by the tensile stress according with buckling. The minute longitudinal cracks induced by shear stress also occurred at the compression zone of the mid-height (Fig. 9(c) and (d)). However, the concrete of specimen SSU-Z-40 exhibited several tiny transverse cracks besides a major one at the tension side of concrete. In addition, a longitudinal tensile crack in concrete extended from the mid-height to the bottom as presented in Fig. 10(c) and (d), and the length of the longitudinal crack was about 380 mm. It further indicated that the outer steel tube had confinement effects on the concrete, which can effectively reduce the development of cracks in the concrete. Simultaneously, the SRCFST members can continue to carry the load after local buckling and failure occurred in the steel tube.

For four eccentrically loaded specimens, i.e. CUS-P50-40, CSU-P80-40, SSU-P50-40 and

SSU-P80-40, the failure modes of the concrete at the tension side were presented in Fig. 11. It can be observed that: (1) the tensile regions, denoted by the distribution of the transverse cracks, extended with the increase of eccentricity; (2) for SRCFST specimens of square cross-section, the width of longitudinal cracks increased with the increase of eccentricity, and the length of longitudinal cracks extended from about 600 mm to 1800 mm (i.e. developing from around maximum lateral deflection to the bottom of column) with an increase of 200% when changing the eccentricity from 50 to 80 mm; (3) the concrete severely cracked in the longitudinal direction for specimen SSU-P80-40 compared with transverse cracks. The observation shows that the eccentricity had marked influences on the failure modes of SRCFST columns.

To better investigate the failure characteristic of the profiled steel after the fire, the outer concrete was removed subsequently. Fig. 12 shows failure modes of the profiled steel, taking specimens CSU-P80-40 and SSU-P80-40 as examples. As expected, both profiled steel exhibited global buckling, which was coincident with overall failure modes of them. The local buckling, posited at the compression region around half of specimen, were observable for flange of profiled steel of SSU-P80-40, as presented in Fig. 12(b), and can be hardly visible for CSU-P80-40. The integrity and small deformation for profiled steel indicating that its resistance to local buckling and overall stability can be improved by reinforcement of outer concrete.

The interface in flange of profiled steel and the outer concrete had detachment to varying degrees, and the longitudinal cracks of the concrete were consistent with the positions of the flange, as illustrated in Fig. 13 (taking SSU-P80-40 as example). It may be ascribed to the accounts that (1) shared axial load were mainly carried by profiled steel and concrete, and were redistributed among each component due to stiffness degradation of steel tube and cracks of outer concrete; (2) reduced confinement effects of steel

tube on outer concrete and softening of outer concrete were occurred at elevated temperature, resulting in uncoordinated lateral deformation between outer concrete and profiled steel; (3) shear stress in contact surface between outer concrete and profiled steel increased as the increase of compressive stress in cross section. Therefore, the interface in outer concrete and the flange of profiled steel exhibited bonding failure in the fire situation, and outer concrete cracked along the flange of profiled steel. Hence, it is recommended to use shear stud for resisting the bond failure of interface between steel and concrete in practice.

The gap in inner interface between profiled steel and core concrete did not occur (in Fig. 14), and the removal of core concrete was arduous. In addition, the visible core concrete presented no evidence of failure. This further confirmed that profiled steel provided great confinement effect to core concrete, which can efficiently suppress the generation and development of cracks in concrete. Therefore, it can be conclude that (1) the overall performance of SRCFST member tended to be dominated by profiled steel and core concrete; (2) the stability and ductility of SRCFST member can be enhanced by profiled steel; (3) inserted profiled steel had significant contribution for resisting fire load.

3.2 Temperature distribution

The average temperature (T) verse time (t) relationships of 25 measurement points in fire furnace agreed well with the ISO-834 standard heating curve, as illustrated in Fig. 15. Several measured data in specimens were missing or invalid, which may be caused by movement or failure of thermocouple end when casting concrete and installing specimen. Hence, they were not listed in follow figures.

Figs. 16-17 present the measured T –t curves of SRCFST columns, where the locations of measurement points were illustrated in subsection 2.4. The evolution in time of the temperature is discussed taking specimen SSU-Z-40 as an example.

The temperature of the measurement points on steel tube, concrete and profiled steel developed progressively with the time. For the steel tube, the temperature of point 11 increased dramatically at the beginning of heating and then slowed down, which coincided with variation tendency of furnace temperature. Nevertheless, the temperature of the measurement points on steel tube were much lower than the average temperature of the fire furnace.

By contrast, the *T-t* relationships of concrete evidently presented lag because of greater heat absorption capacity and lower thermal conductivity. It is noticed that the *T-t* curves of concrete (points 5 and 10) exhibit a plateau or gradual temperature rise of concrete lasting for 10 min from the beginning of test. It is difference to retain temperature stabilized of whole concrete section in a short time, caused by poor performance of heat transfer according to [32]. Since the concrete in point 5(10) was heated more quickly after 10min. It is noteworthy that an evident plateau in the *T-t* curves of point 5(10) can be observed at about 100°C. For instance, the plateau in the *T-t* curves of point 5 ranged from 102°C to 103°C after heated for 29 min, lasting about 11min. Similarly, the *T-t* curves of specimens CSU-Z-40 and SSU-Z-50 exhibited plateau stage range of 102°C to 109°C from approximately 40min, lasting for 7-11min. The reason for above is that the evaporation and migration of free water in the concrete take away part of the heat in the specimen.

Obviously, the temperature rise of profiled steel leg behind that of the surface of steel tube significantly, which was attributed to protection of insulate concrete. The temperature of the measurement points 2 and 4 were almost identical with that of point 3 during the entire test, and were 233.3°C, 259.8°C and 257.1°C at the end of fire exposure, respectively. By contrast, the temperature attainted by point 1 was lower than that of measurement points mentioned above, and was 189.5°C at 74min. The reason why the temperature difference of approximately 44 to 70 °C existed between flange and web of profiled steel

is that the distance from the centre of web to the fire source was greater than those from the flange. Suddenly slow increases or inflection point in *T-t* curves of profiled steel were observed, after heated for 7 to 11 min. Correspondingly, the temperature of the profiled steel was approximately 100℃. This is related to evaporation of moisture in concrete around profiled steel. However, the temperature of profiled steel increased more quickly than that of measurement points in concrete. For example, the temperature of point 5 and 10 at 44.5min (thermocouple of point 5 was failure after 44.5min) were 131.3℃ and 124.3℃ respectively, with a temperature difference of approximately 50 ℃ compared to measurement point 1, and simultaneously, the temperature difference ranged of 30 to 70 ℃ were captured for rest specimens at the end of fire exposure. This may be because (1) much greater heat conductivity for profiled steel although surrounded by concrete, and (2) profiled steel was heated via cracks in concrete besides surrounded concrete.

In theory, the temperature attained by steel tube up to above 400℃, had significant influence on the elasticity modulus and strength of steel, which dramatically reduced [32] as the increase of temperature. For the tested specimens, the temperature of concrete and profiled steel were less than 280℃, indicating that the strength properties of both concrete and profiled steel had limited effect. Therefore, it can be inferred that the profiled steel had significant contributions to the load carrying capacity of SRCFST members in the fire situation.

To examine the variations of temperature field along the longitudinal direction, the maximum temperature attained by measurement point 11 and 12 were compared, and the little higher temperature of point 11 at mid-height than point 12 at bottom of columns for all specimens were noticed in Fig. 18 (for simplicity, the X-axis corresponded to the number of specimens in Table.1). This may be related to relatively major heat accumulation in the upper part of the furnace cavity. CSU-P50-40 exhibited the

maximum temperature difference up to 34.2℃ with an error of 6.68%. Therefore, it can be deemed that the surface temperature is uniform along the longitudinal direction of specimens.

3.3 Deformation and fire resistance

The measured axial deformation versus time relationships were shown in Fig. 19. The displacement of the deformation at ambient temperature was deducted from the test results. Time-displacement velocity curves, obtained via taking the slope of measured axial deformation, was also presented in Fig.19. For simplicity, axial deformation-time curves and rate of axial contraction-time curves shared the same horizontal axis. Note that the curves in the figure all took the manual ignition time of the fire furnace as the starting point, and elongation was taken as positive and shortening negative.

For SRCFST columns with small load ratio *n*, i.e. specimens CSU-Z-40 and SSU-Z-40, the development of axial deformation goes through five stages as presented in Fig. 20, that is, expansion deformation in the early stage (OA), steady increase of compression deformation stage (AB), deformation recovery stage (BC), an again shortening stage (CD) and accelerated failure stage (DE), which is consistent with that of CFST columns with solid steel core [25]. Taking specimen SSU-Z-40 as example, stage OA lasts 10min reaching a peak expansion deformation of 1.74 mm. During this stage, the deformation of SRCFST columns is mainly determined with the thermal expansion of the steel tube. The specimens of circular cross-section featured a smaller peak expansion deformation. The compression deformation levels off in AB stage (10 to 23 min). The temperature of steel tube reached over 500℃ after heating 23 min (based on Fig. 17). Then, the axial deformation featured a second increasing stage, BC, which lasted 20 min with a maximum expansion deformation of 1.73 mm. The specimen CSU-Z-40 showed a smaller maximum expansion of 1.49 mm in BC stage. With the ongoing heating, the axial deformation started to shorten again because the deterioration of materials induced by fire exceeded the

thermal expansion. Finally, the axial deformation dramatically increased to failure in DE stage.

For the specimens with high load ratio (n>0.4) and eccentric load, the axial deformation versus time curves can be divided into three stage, i.e. initial expansion stage (OA′), compression stage (A′D′) and an accelerated failure stage (D′E′), which is consistent with that of CFST columns [35]. The same conclusions have been obtained by FE analysis for SRCFST columns in reference [36]. Note that the axial deformation versus time curves featured a tendency of slow growth at 14 min, and the axial compression rate curve changed abruptly, as showed in Fig. 19(d). This is because load increased transitorily, resulting in unexpected compression at the moment.

When the specimens were about to reach the fire resistance, and axial deformation tended to increase dramatically and it was difficult to maintain the load. For specimens CSU-Z-40, CSU-Z-50, SSU-Z-40 and SSU-Z-50, failure would certainly be attained if the loading rate would be able to catch up, although both the axial deformation and deformation rate were not reached failure criteria stated in subsection 2.5. Therefore, the end time of the fire experiment was identified as the actual fire resistance of test specimen.

Fig. 21 shows the lateral displacement versus time relationship of SRCFST columns. It is worth noting that lateral displacement in the tension zone for specimens CSU-Z-40, SSU-Z-40 and SSU-Z-50 are presented in Fig. 21, and the lateral displacement for rest of specimens at the compression area are measured. The reason why the directions of lateral displacement are inconsistent is that the deflection direction for axially loaded specimens is unpredictable due to initial imperfection. The tendency of lateral displacement versus time curves in compression area is similar to axial deformation analysed above, and can be generally divided into three stages, i.e. the expansion stage, the compression stage, and the failure stage.

4. Discussion of the experimental results

4.1 Critical temperatures

This subsection focuses on the critical temperature for the tested SRCFST columns. Similar to the definition of the critical temperature of steel members, T_{cr} is defined herein as the critical temperature of SRCFST columns, which can be attained by the surface of the steel tube when the SRCFST column reaches the fire resistance.

In previous research on structural fire design, it is clearly found that the fire resistance of steel components can be determined in the temperature domain, and the applicability to CFST members were confirmed [37-40]. Branching from CFST members, the fire resistance of SRCFST members could be dependent on the critical temperature of steel tube. According to the measured results of the temperature field (Fig. 18), the critical temperature of the outer steel tube were 684.9 °C for SSU-Z-40 (load ratio n=0.40) and 623 °C for SSU-Z-50 (n=0.49), respectively. The critical temperature of steel component for a uniform temperature distribution may be determined for load ratio, and decrease with the increase of load ratio.

Both Eurocode 3 [41] and AS4100 [42] give calculation formulas on critical temperature of steel structures, and the critical temperature is related to the load ratio only. The critical temperatures of specimens SSU-Z-40 and SSU-Z-50 are compared with the critical temperatures in the specification, as shown in Fig.22. When the same load ratios of the specimens in the experiments were used, the critical temperatures calculated by EC3 and AS4100 were 620 to 588 °C and 631 to 545 °C, respectively, which is significantly lower than the ultimate temperature of the composite column. It indicates that when the surface temperature of the steel tube rises to the critical temperature of steel, the material properties are degraded and cannot continue to work properly. The load on the steel tube is internally transferred, and is

redistributed among each components, so that the SRCFST columns can continue to bearing.

A formula to predict the critical temperature of the steel tube surface were proposed according to GB 50936-2014 [28] and AIJ [43] when the CFST column reaches the fire resistance. Fig. 23 illustrated the comparison of the measured critical temperature with the calculated values. The critical temperature of the steel tube surface considers the combined influence of wall thickness and heating time in GB50936-2014 [28], but only considers the influence of heating time on steel tube temperature in AIJ [43]. Obviously, the measured critical temperature T_{cr} of outer steel tube are much lower than calculated results according to GB 50936-2014 [28], and the similarities were observed for results obtained by AIJ [43] except specimen SSU-P80-40. The measured critical temperature T_{cr} for specimen CSU-Z-50 was 516.6°C, and were 616.1°C and 569.4°C respectively under same heating time and cross-section dimension according to GB 50936-2014 and AIJ, with a temperature difference of 99.5°C and 52.8°C respectively. In addition, the temperature difference of T_{cr} between measured and predicted results progressively increases with the heating time. This is may be related to embedded profiled steel. The cross-section area of concrete for CFST members is greater than that of SRCFST columns under the same cross-section parameters due to profiled steel, resulting in greater thermal properties. Additional, the shared load can be redistributed among three components, i.e. outer steel tube, concrete and profiled steel for SRCFST members when outer steel tube cannot resist load subjected to high temperature. In general, the contribution of profiled steel improve the fire performance.

4.2 Fire resistance

4.2.1 Influence of load ratio

The influence of load ratio *n* on the axial deformation of SRCFST specimens is shown in Fig. 24(a). It can be observed that load ratio *n* has a significant influence on axial deformation of SRCFST columns.

Both peak expansion deformation and the corresponding time are generally reduced with the increase of *n*. For example, the peak expansion deformation of 1.49 mm is reached for specimen CSU-Z-40 at about 20 min, and 1.24 mm for specimen CSU-Z-50 at 10 min. In addition, the failure stage (C-D) is affected by *n*. For specimen with high load ratio (n>0.4), the axial deformation-time (t) curves dramatically decrease after point C, but the axial deformation of specimens with lower load ratio ($n \leq 0.4$) are relatively smooth at the accelerated failure stage.

Obviously, the fire resistance of SRCFST columns decrease with the increase of load ratio *n*, as shown in Fig. 24(b). When *n* increased from 0.40 to 0.52, the fire resistance of circular SRCFST columns decreased from 70 to 23min with a decrease of 67%. Similarly, the fire resistance of square SRCFST columns decreased by 35% when the load ratio increased from 0.39 to 0.49. The material properties degrade at elevated temperature, especially steel, and the thermal strain caused by temperature and the stress induced strain both increase gradually. When the load level is high, the specimen is more likely to attain the ultimate level of stress induced strain, and the failure to the specimen comes earlier.

4.2.2 Influence of eccentricity

Loading eccentricity has evident influences on axial deformation of SRCFST members, as presented in Fig. 25. It can be observed that with the increases of eccentricity, (1) the peak expansion deformation and corresponding heating time decreased, and (2) the limit axial contraction increased. In addition, for the specimens under concentric compression, taking CSU-Z-40 as an example, the axial deformation develop after 56 min (the compression stage) until the failure occurred. Although the specimen has imperfections, such as an initial eccentricity or an initial bending according to above, it does not show obvious brittle failure. By contrast, the axial deformation of eccentrically loaded specimens suddenly decreased at the compression stage, and the specimen deformed rapidly, which shows typical instability

and failure mode of the eccentric columns. The reason is that the effect of the second-order effect of the bending moment generated by the eccentric load is enhanced significantly for specimen with larger eccentricity, and the axial deformation increases as well. The influences of eccentricity for the SRCFST specimens of square cross-section are consistent with the SRCFST specimens of circular cross-section.

When the eccentricity increased from 0 to 50 or 80 mm, the fire resistance of SRCFST columns significantly decreased, as presented in Fig. 26. The fire resistance of specimens CSU-P50-40 and CSU-P80-40 are 31 and 19 min respectively, which decrease by 56% and 73% respectively compared to specimens CSU-Z-40. For eccentrically loaded specimens, although the fire resistance decrease when eccentricity changes from 50mm to 80mm, the fire load of corresponding specimens also increase. For eccentrically loaded SRCFST specimens in this paper, the influences of eccentricity on fire resistance are complicated combined load ratio mentioned in subsection 4.2.1, thus the details of eccentricity should be further studied

4.3 Assessment of fire resistance

Various design method have been proposed for fire engineering design of CFST columns. However, there is no special design method to calculate the fire resistance time of SRCFST columns. Branching from the CFST columns, the applicability of fire resistance design methods for SRCFST columns should be further evaluated.

A simplified method to predict the fire resistance of steel-concrete composite columns was recommended in EN 1994-1-2 [44], whereas mostly on both totally and partially encased steel sections and concrete filled hollow sections. GB 50936-2014 [28] specifies the tabulated data for fire resistance time of CFST columns, which does not involve the any calculation. Meanwhile, the calculation method in GB 50936-2014 calculates the bearing capacity of CFST columns under the fire, and the fire resistance

time can be determined by means of repeated iteration and trial calculation. Hence, it is relatively complicated. Han [33] provides design method of CFST columns under ISO-834 standard fire exposure. Simultaneously, the fire resistance time of composite columns can be gained according to calculating formulas of critical temperature mentioned on subsection 4.1. An overview on evaluation of design method is outlined in this study, which will be design guides of fire resistance on SRCFST columns.

4.3.1 *Eurocode* (EN 1994-1-2)

The design resistance of composite columns under axial compression should be obtained from *Eqs*.(1) according to EN 1994-1-2.

$$N_{fi,Rd} = \chi N_{fi,pl,Rd} \tag{1}$$

where $N_{fi,pl,Rd}$ is the design value of the plastic resistance to axial compression in the fire situation, which can be obtained by *Eqs*.(2); and χ is the reduction coefficient for buckling curve of Eurocode 3 and depending on the relative slenderness. Three components, i.e. steel tube, concrete and profiled steel are divided for SRCFST columns, and which are denoted "a", "c" and "s" respectively in *Eqs*.(2).

$$N_{fi,pl,Rd} = \sum_{f}(A_{a,\theta} f_{ay,\theta}) / \gamma_{M,fi,a} + \sum_{k}(A_{s,\theta} f_{sy,\theta}) / \gamma_{M,fi,s} + \sum_{m}(A_{c,\theta} f_{cy,\theta}) / \gamma_{M,fi,c} \tag{2}$$

where $A_{i,\theta}$ is cross-sectional area of each element at a certain temperature θ. $\gamma_{M,fi,i}$ is partial factor for a material property in the fire situation, which are taken as 1.0 in this paper.

The effective flexural stiffness can be obtained from:

$$(EI)_{fi,eff} = \sum_{j}(\varphi_{a,\theta} E_{a,\theta} I_{a,\theta}) / \gamma_{M,fi,a} + \sum_{k}(\varphi_{s,\theta} E_{s,\theta} I_{s,\theta}) / \gamma_{M,fi,s} + \sum_{m}(\varphi_{c,\theta} E_{c,\sec,\theta} I_{c,\theta}) \tag{3}$$

where $I_{i,\theta}$ is the second moment of area of the partially reduced part i for bending around the weak or strong axis. $E_{c,\sec,\theta}$ is the characteristic value for the secant modulus of concrete infill in the fire situation, determined by EN 1994-1-2. $\varphi_{i,\theta}$ is the reduction coefficient based on the effect of thermal stresses. Note that the temperature distribution in the cross-section should be obtained firstly. Additional, the simplified method given in EN 1994-1-2[44] are merely applicable in columns subjected to axial load.

4.3.2 *Chinese code* (GB 50936-2014)

GB 50936-2014[28] propose the design methods for CFST columns exposed to fire conditions. It allows the use of simple calculation method for resistance and a simple calculation equation for critical temperature. The design method for resistance calculates the bearing capacity at different heating time based on average temperature in concrete and steel tube, which is similar to the method for bearing capacity at ambient temperature. Similar to simplified model in subsection 4.3.1, the design method for resistance in GB 50936-2014[28] caters for composite columns subjected to axial compression only.

The simple methods for predicting the ultimate temperature (i.e. critical temperature) for steel tube surface of CFST columns, as shown in *Eqs*.(4-7), which are relative to the heating time of composite columns. Based on measured critical temperature of SRCFST specimens, the fire resistance of SRCFST specimens are calculated employing *Eqs*.(4-7), and are compared with experimental results.

$$T_{\mathrm{cr}} = A\left(1-\frac{1}{1+\left(\frac{t}{B}\right)^{C}}\right)+20 \tag{4}$$

$$A = 1200 \tag{5}$$

$$B = 20.22 + 0.51t_{\mathrm{s}} \tag{6}$$

$$C = 0.996 + 0.014t_{\mathrm{s}} \tag{7}$$

where t_{s} is equivalent thickness of steel tube(mm), which can be equivalent to a circle according to its areas for square steel tube. t is heating time(h).

Additional, the fire resistance time of CFST columns, based on external diameter of steel tube and load ratio, can be obtained according to the tabular data, which provides a relatively more straightforward guide on fire resistance time of CFST columns.

4.3.3 A regression formula according to FEA by Han

Han [33] provides a regression formula according to FEA for calculating the residual strength index of CFST columns. There is a corresponding fire duration for a given residual strength index (the ratio between ultimate bearing capacity at ambient temperature and under the fire), which is the fire resistance time under the corresponding load ratio. This equation is suitable for eccentricity ratio (e/r) 0-3, concrete with cubic strength 30MPa-90MPa, steel yield strength 200MPa-500MPa, steel tube ratio 0.03-0.2 and slender ratio 10-120.

4.3.4 *Japanese code* (AIJ)

In place of calculation fire resistance time, the Japanese code AIJ [43] calculates the critical temperature on the steel tube of CFST columns based on the *Eq*. (8), which depends on the heating time only. Therefore, the fire resistance time can be determined based on measured temperature showed in Fig.18.

$$T_{cr} = 1080 - 450\,exp(-0.8t) - 630\,exp(-3t) + 20 \tag{4}$$

where t is heating time(h).

4.3.5 Evaluation of fire resistance time

The tested fire resistance of Eight SRCFST specimens is evaluated by above design methods, and the summary of tested fire resistance and predicted results are tabulated in Table. 4, and compared in Fig. 27. The fire resistance obtained from test is t^{exp} in Table 4, and fire resistance time predicted using simplified method in EN 1994-1-2, tabulated data in GB 50936-2014[28], calculation method in GB 50936-2014[28], regression formula by Han, the calculation equation of critical temperature in GB 50936-2014[28] and AIJ[43] can be expressed with t_{EC4}, $t_{GB,Table}$, t_{GB}, t_{Han}, $t_{GB,Tcr}$ and $t_{AIJ,Tcr}$ respectively.

It can be clearly seen that predicted fire resistance are conservative compared with test results. The simplified method in EN 1994-1-2[44] underestimates the fire resistance of SRCFST specimens with 20%

in average because it is applicable for the composite columns including SRCFST columns. The design methods applied for CFST columns, i.e. tabulated data in GB 50936-2014[28], calculation method in GB 50936-2014[28], regression formula by Han, the calculation equation of critical temperature in GB 50936-2014[28] and AIJ[43], provide the conservative predictions respectively with 34%, 16%, 28%, 67% and 54% in average.

For axially loading SRCFST columns, calculation method in GB 50936-2014[28] provides the closest predictions of fire resistance although safely underestimate the fire resistance by 16% in average. The predicted fire resistance by EN 1994-1-2[44] are close to that by calculation method in GB 50936-2014[28] but has an unsafe prediction for specimen CSU-Z-50. Compared with tabulated data in GB 50936-2014[28] and regression formula by Han and the calculation equation of critical temperature in AIJ[43], calculation equation of critical temperature in GB 50936-2014[28] provide the more safe predictions for SRCFST specimens subjected to eccentric compression, but underestimates the fire resistance of SRCFST columns over 30% with the exception of specimen SSU-P80-40. Tabulated data in GB 50936-2014[28] and regression formula by Han overpredict the fire resistance for all eccentric compressive SRCFST columns because they assume effect of eccentricity on fire resistance of CFST columns is limit. Meanwhile, calculation equation of critical temperature in both AIJ[43] and GB 50936-2014[28] ignore the negative influence of load ratio, eccentricity, slender ratio on fire resistance.

Thus, there is no applicable calculation method to accurately and safely predict the fire resistance of all SRCFST specimens. Calculation method in GB 50936-2014[28] provides the safe predictions for axially-loaded SRCFST columns, but the accuracy of predictions should be further improved. It is necessary to further investigate the fire design method for SRCFST columns, which needs to consider the effect of various factors on fire resistance comprehensively.

5. Conclusions

The experimental investigation for SRCFST columns under the ISO-834 standard fire are carried out to study the fire performance and response in this paper. A total of eight SRCFST columns, focusing on various test parameters of form of cross-section, fire load ratio, eccentricity are performed. Based on the observations and discussion of experimental results, the following conclusions can be drawn:

(1) All specimens presented global buckling after failure. The local failure modes were affected by load ratio and eccentricity. The visible core concrete presented no evidence of failure and cracks, the slight local buckling in profiled steel can be observed due to restraint of concrete. It indicates that profiled steel provided great confinement effect to core concrete, and can efficiently suppress the generation and development of cracks in concrete. The maximum temperature attained by profiled steel was less than 280℃ in current test, indicating significant contribution of profiled steel for resisting fire load.

(2) Without fire protection, SRCFST columns under concentric and eccentric compression exhibited the excellent fire resistance although it did not achieve the fire rating. For the axially loaded specimens with high load ratio (n>0.4) or specimens under eccentric compression, the fire resistance ranged from 14-48min, it is essential to do fire protection on them.

(3) The load ratio is a significant factor affecting the fire resistance and axial deformation of SRCFST columns. For specimens with common load ratio (n=0.4, the actual load ratio n were less than 0.4), the axial deformation versus time curves underwent five stages, i.e. expansion stage, steady increase of compression deformation stage, deformation recovery stage, an again shortening stage and accelerated failure stage, which is differ from that of SRCFST specimens with eccentric load and high load ratio (n>0.4)

(4) Critical temperature on surface of steel tube is much lower compared with CFST columns at

same exposure time. Simultaneously, the tested fire resistance of SRCFST columns were higher than CFST columns with same parameters, with an improvement of 55% under common load ratio. It indicates that the load redistribution occurred in the component during the fire, and embedded profiled steel for SRCFST columns has significant enhancement for fire performance.

(5) The current design method applied to CFST columns and SRCFST columns were estimated with the test fire resistance of eight SRCFST specimens. The simplified method in EN 1994-1-2 underestimates the fire resistance of SRCFST specimens and is unsafe for all SRCFST specimens. Calculation method in GB 50936-2014 provides the closest predictions for axially-loaded SRCFST columns, but it is not applicable for SRCFST specimens subjected to eccentric load. Tabulated data in GB 50936-2014 and regression formula by Han is unsafe for eccentrically-loaded SRCFST specimens and overconservative for axially-loaded SRCFST specimens. Overall, further investigation on design method of SRCFST columns is needed to consider the effect of various factors on fire resistance comprehensively.

Acknowledgements

This research reported in this paper is the projects supported by National Natural Science Foundation of China (No. 51778274; 51468037). The authors would like to express their sincere appreciation to these supports.

References

[1] Kato Ben. Column Curves of Steel-concrete Composite Members. J Constr Steel Res 1996; 39 (2): 121-135.

[2] Wang JH, He J, Xiao Y. Fire behavior and performance of concrete-filled steel tubular columns: Review and discussion. J Constr Steel Res 2019; 157: 19-31.

[3] EN 1994-1-1. Design of composite steel and concrete structures, Part 1.1, general rules and rules for buildings. European Committee for Standardization: Brussels, Belgium; 2004.

[4] Wang QX, Zhao DZ, Guan P. Experimental study on the strength and ductility of steel tubular columns filled with steel-reinforced concrete. Eng Struct 2004; 26:907-915.

[5] Zhu MC, Liu JX, Wang QX, Feng XF. Experimental research on square steel tubular columns filled with steel-reinforced self-consolidating high-strength concrete under axial load. Eng Struct 2010; 32(8): 2278-2286.

[6] Ding FX, Zhang T, Liu XM, Guo Q, Jiang GS. Behavior of steel-reinforced concrete-filled square steel tubular stub columns under axial loading. Thin-Walled Struct 2017; 119: 737-748.

[7] Chang X, Wei YY, Yun YC. Analysis of steel-reinforced concrete-filled steel tubular (SRCFST) columns under cyclic loading. Constr Build Mater 2012; 28: 88-95.

[8] Farajpourbonab E, Kute SY, Inamdar VM. Steel-reinforced concrete-filled steel tubular columns under axial and lateral cyclic loading. Int J Advanced Struct Eng 2018; 10: 61-72.

[9] Shi YL, Xian W, Wang WD, Li HW. Mechanical behaviour of circular steel-reinforced concrete-filled steel tubular members under pure bending loads. Struct 2020; 25: 8-23.

[10] Shi YL, Xian W, Wang WD, Li HW. Experimental performance of circular concrete-filled steel tubular members with inner profiled steel under lateral shear load. Eng Struct 2019; 201: 109746.

[11] Xian W, Wang WD, Wang R, Chen WS, Hao H. Dynamic response of steel-reinforced concrete-filled circular steel tubular members under lateral impact loads. Thin-Walled Struct 2020; 151: 106736.

[12] Wang WD, Jia ZL, Shi YL, Tan EL. Performance of steel-reinforced circular concrete-filled steel tubular members under combined compression and torsion[R]. J Constr Steel Res 2020; 173:

106271.

[13] Wang WD, Xian W, Hou C, Shi YL. Experimental investigation and FE modelling of the flexural performance of square and rectangular SRCFST members. Struct 2020; 27: 2411-2425.

[14] Lie TT, Chabot M. Experimental studies on the fire resistance of hollow steel columns filled with plain concrete. NRC-CNRC Internal Report, 1992, No.611.

[15] Kodur VKR. Performance-based fire resistance design of concrete-filled steel columns. J Constr Steel Res 1999; 51: 21-36.

[16] Romero ML, Moliner V, Espinos A, Ibañez C, Hospitaler A. Fire behavior of axially loaded slender high strength concrete-filled tubular columns. J Constr Steel Res 2011; 67: 1953-65.

[17] João PC, Rodrigues, Luís L. Fire resistance of restrained composite columns made of concrete filled hollow sections. J Constr Steel Res 2017; 133: 65-76.

[18] Espinos A, Romero ML, Hospitaler A. Advanced model for predicting the fire response of concrete filled tubular columns. J Constr Steel Res 2010; 66(8): 1030-1046.

[19] Han LH, Yang YF, Xu L. An experimental study and calculation on the fire resistance of concrete-filled SHS and RHS columns. J Constr Steel Res 2003; 59(4): 427-452.

[20] Espinos A, Romero ML, Lam D. Fire performance of innovative steel-concrete composite columns using high strength steels. Thin-Walled Struct 2016; 106: 113-128.

[21] Tan QH, Gardner L, Han LH, Song TY. Fire performance of steel reinforced concrete-filled stainless steel tubular (CFSST) columns with square cross-sections. Thin-Walled Struct 2019; 143: 1-15.

[22] Zhu MC, Meng FQ, He BJ. Experimental research on fire resistance of steel tubular columns filled with steel reinforced concrete. J Build Struct 2016; 37(3): 36-43.

[23] Meng FQ, Zhu MC, Mou B, He BJ. Residual strength of steel-reinforced concrete-filled square steel

tubular (SRCFST) stub columns after exposure to ISO-834 standard fire. Int J Steel Struct 2019; 19(3): 850-866.

[24] Neuenschwander M, Knobloch M, Fontana M. Modeling thermo-mechanical behavior of concrete-filled steel tube columns with solid steel core subjected to fire, Eng Struct 2017; 136: 180-193.

[25] Neuenschwander M, Knobloch M, Fontana M. ISO standard fire tests of concrete-filled steel tube columns with solid steel core. J Struct Eng 2017; 143(4): 04016211.

[26] Klingsch W. Analyse des tragverhaltens von geilinger baustützen bei normaltemperatur und bei brandbeanspruchung sowie der zughörigen bemessungsverfahren. Wuppertal, Germany: Bergisch universität Wuppertal Gutachten; 1984.

[27] Schaumann P, Kleibömer I. Thermal and structural response of concrete-filled tubular columns with massive steel core in case of fire. Bautechnik 2015; 92(5): 330-334.

[28] GB 50936-2014. Technical code for concrete filled steel tubular structures. China Architecture &Building Press: Beijing, China; 2014.

[29] JGJ138-2016.Code for design of composite structures. 2016, China Architecture &Building Press: Beijing, China.

[30] YB 9082-2006. Technical specification of steel-reinforced concrete structures. 2006, Metallurgical industry press: Beijing, China.

[31] ISO 834-1: 1999. Fire-resistance tests-elements of building construction-Part 1: General requirements. International organization for standardization, Geneva; 1999.

[32] Li GQ, Han LH, Lou GB, Jiang SC. Fire safety design of steel and steel-concrete composite structures. Architecture &Building Press: Beijing, China; 2006.

[33] Han LH. Concrete Filled Steel Tubular Structures-Theory and Practice, 3rd ed. Science press: Beijing, China; 2016.

[34] Zhong ST. The continuity of axial compressive behaviors of concrete filled steel tube (CFST) for circular, octagonal, square and rectangular forms. Prog Steel Build Struct 2004; 6(2): 14-22.

[35] Hong SD. Varma AH. Analytic modeling of the standard fire behavior of loaded CFT columns. J Constr Steel Res 2009; 65: 54-69.

[36] Mao WJ, Wang WD, Xian W. Numerical analysis on fire performance of steel-reinforced concrete-filled steel tubular column with square cross-section. Struct 2020; 28: 1-16.

[37] Kodur. Performance of high strength concrete-filled steel columns exposed to fire. Can J Civil Eng 1998; 25(6): 975-981.

[38] Han LH, Zhao XL, Yang YF, Feng JB. Experimental study and calculation of fire resistance of concrete-filled hollow steel columns. J Struct Eng 2003; 129(3): 346-356.

[39] Lu H, Han LH, Zhao XL. Fire performance of self-consolidating concrete filled double skin steel tubular columns: Experiments. Fire Safety J 2010; 45: 106-115.

[40] Wang YC. The effect of structural continuity on the fire resistance of concrete filled columns in non-sway frames. J Constr Steel Res 1999; 50(2): 177-197.

[41] EN 1993-1-2. Design of steel structures-Part 1.2: General rules-Structural fire design. European Committee for Standardization: Brussels, Belgium; 2005.

[42] AS4 100. Steel structures. Standards Australia: Sydney, NSW; 1998.

[43] AIJ. Recommendations for design and construction of concrete filled steel tubular structures. Architectural Institute of Japan (AIJ): Tokyo, Japan; 2008.

[44] EN 1994-1-2. Design of composite steel and concrete structures-Part 1-2: General rules-Structural

fire design: Brussels, Belgium; 2005.

Nomenclature

A_c	concrete cross-sectional area
A_{st}	steel tube cross-sectional area
A_{ss}	profiled steel cross-sectional area
t	wall thickness of steel tube or fire during time
H	length of the composite column
n	load ratio, $n = N_F / N_u$
h	height of I section profiled
b	flange width of I section profiled
d	web thickness of I section profiled
t_w	flange thickness of I section profiled
N_F	constant load applied on the column in test
N_u	ultimate bearing capacity of column at ambient temperature
α_{st}	steel tube ratio, $\alpha_{st} = A_{st}/A_c$
α_{ss}	profiled steel ratio, $\alpha_{ss} = A_{ss}/A_c$
e/r	eccentricity ratio
f_{cu}	concrete cubic compressive strength
f_y	yield strength of steel
f_u	ultimate strength of steel
f_{ck}	characteristic concrete strength

E_s	modulus of elasticity of steel
μ_s	Poisson' ratio of steel
δ_{10}(%)	elongation
T_{cr}	critical temperature
t_R	fire resistance
t^{exp}	fire resistance obtained from test
t_{EC4}	fire resistance predicted using simplified method in EN 1994-1-2
$t_{GB,Table}$	fire resistance predicted using tabulated data in GB 50936-2014
t_{GB}	fire resistance predicted using calculation method in GB 50936-2014
t_{Han}	fire resistance predicted using regression formula by Han
$t_{GB,Tcr}$	fire resistance predicted using the calculation equation of critical temperature in GB 50936-2014
$t_{AIJ,Tcr}$	fire resistance predicted using the calculation equation of critical temperature in AIJ

Tables

Table 1 Summary of specimen information

No.	Specimen label	Dimensions of tube (mm)	Profile steel	Steel tube ratio	Profile steel ratio	Load eccentricity(mm)	Load ratio	Load (kN)	Fire resistance(min)
1	CSU-Z-40	325×6	A	0.068	0.046	0	0.40	2212	70
2	CSU-Z-50	325×6	A	0.068	0.046	0	0.52	2900	23
3	CSU-P50-40	325×6	A	0.068	0.046	50	0.40	1410	31
4	CSU-P80-40	325×6	A	0.068	0.046	80	0.46	1300	19
5	SSU-Z-40	300×5.5	B	0.082	0.056	0	0.39	2404	74
6	SSU-Z-50	300×5.5	B	0.082	0.056	0	0.49	3000	48
7	SSU-P50-40	300×5.5	B	0.082	0.056	50	0.42	1672	28
8	SSU-P80-40	300×5.5	B	0.082	0.056	80	0.46	1500	14

Table 2 Material properties of steel

Materials	f_y(MPa)	f_u(MPa)	E_s(GPa)	μ_s	δ_{10}(%)
Circular steel tube	345	455	193	0.29	35
Plane of squarer steel tube	326	458	181	0.29	41
Corner of squarer steel tube	354	558	179	0.28	14
Steel plane-5mm	277	420	174	0.29	37
Steel plane -8mm	261	412	155	0.29	40

Table 3 Details about apparent characteristics of steel tube for fire resistance test

NO.	Specimen label	T_{max}(℃)	Apparent characteristics (cool completely)
1	CSU-Z-40	676	black grey, oxide layers was partially swollen and falling off
2	CSU-Z-50	517	grey brown and tarnish
3	CSU-P50-40	533	
4	CSU-P80-40	448	dark red
5	SSU-Z-40	685	black grey, oxide layers was partially swollen and falling off
6	SSU-Z-50	655	
7	SSU-P50-40	556	grey brown and tarnish
8	SSU-P80-40	424	dark red

Table 4 Predicted fire resistance for SRCFST specimens

Specimen label	Dimensions of tube (mm)	Load eccentricity(mm)	Load ratio	t^{exp} (min)	t_{EC4}(min) (t^{exp}/t_{EC4})	$t_{GB,Table}$ (min) ($t^{exp}/t_{GB,Table}$)	t_{GB}(min) (t^{exp}/t_{GB})	t_{Han}(min) (t^{exp}/t_{Han})	$t_{GB,Tcr}$ (min) ($t^{exp}/t_{GB,Tcr}$)	$t_{AIJ,Tcr}$ (min) ($t^{exp}/t_{AIJ,Tcr}$)
CSU-Z-40	325×6	0	0.40	70	48(1.46)	32(2.21)	49(1.43)	31(2.26)	29(2.39)	32(2.22)
CSU-Z-50	325×6	0	0.52	23	27(0.85)	23(1.01)	21(1.10)	26(0.88)	18(1.28)	20(1.18)
CSU-P50-40	325×6	50	0.40	31	—	32(0.98)	—	31(1.00)	19(1.64)	21(1.51)
CSU-P80-40	325×6	80	0.46	19	—	27(0.71)	—	28(0.68)	14(1.32)	16(1.21)
SSU-Z-40	300×5.5	0	0.39	74	55(1.35)	31(2.41)	70(1.06)	33(2.24)	30(2.47)	33(2.27)
SSU-Z-50	300×5.5	0	0.49	48	42(1.14)	26(1.86)	46(1.05)	27(1.78)	27(1.76)	30(1.61)
SSU-P50-40	300×5.5	50	0.42	28	—	28(1.00)	—	31(0.90)	19(1.46)	21(1.33)
SSU-P80-40	300×5.5	80	0.46	14	—	27(0.52)	—	29(0.48)	13(1.07)	14(0.97)
Average					1.20	1.34	1.16	1.28	1.67	1.54
Std.dev					0.27	0.72	0.18	0.70	0.51	0.48

Figures

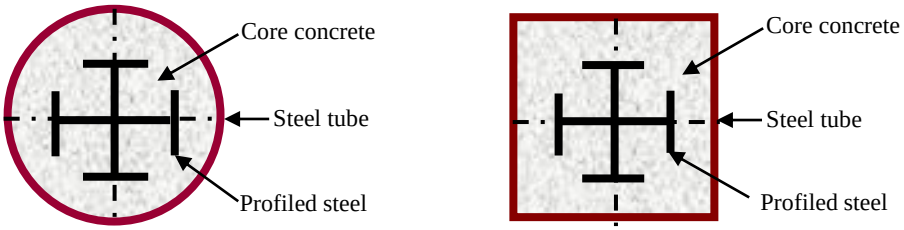

(a) Circular cross-section (b) Square cross-section

Fig.1. Typical cross-sections of SRCFST members.

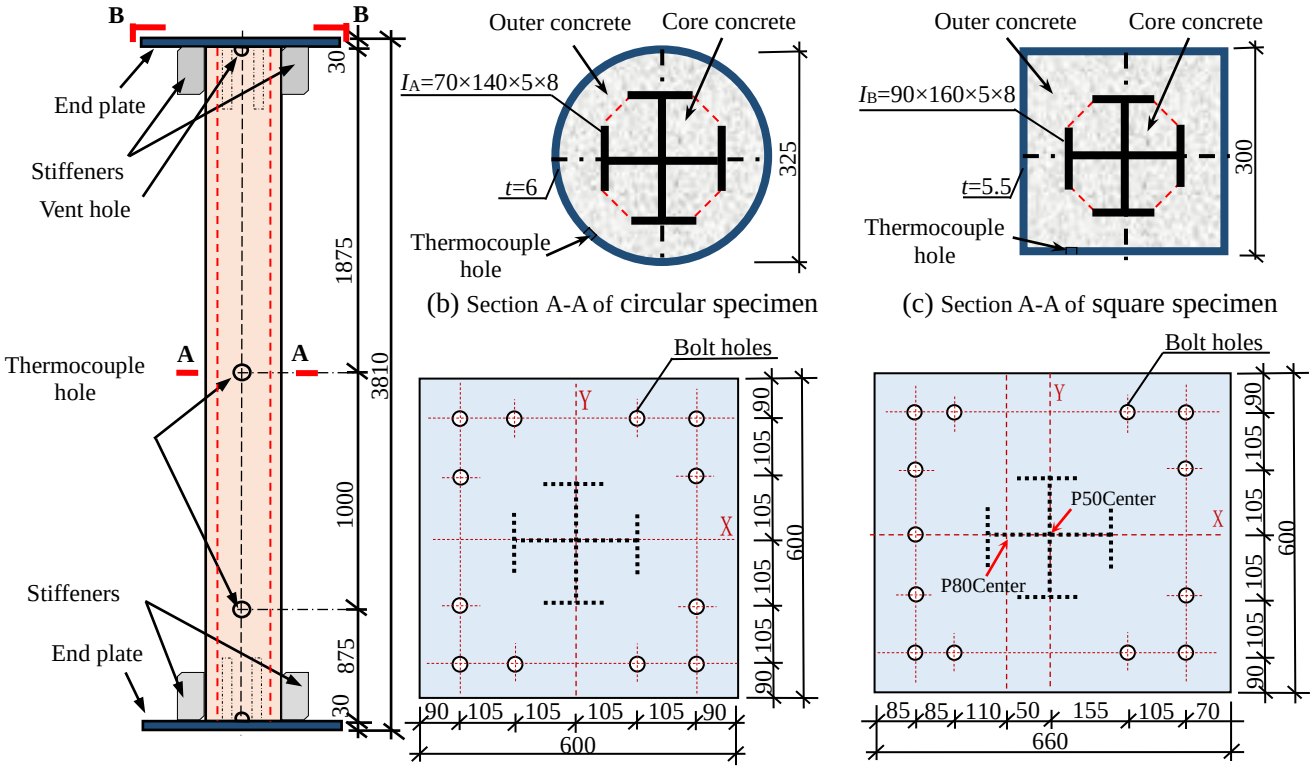

(a) Elevation (b) Section A-A of circular specimen (c) Section A-A of square specimen

(d) Section B-B of axial compression (e) Section B-B of eccentric compression

Fig.2. Details of the specimens (units in mm)

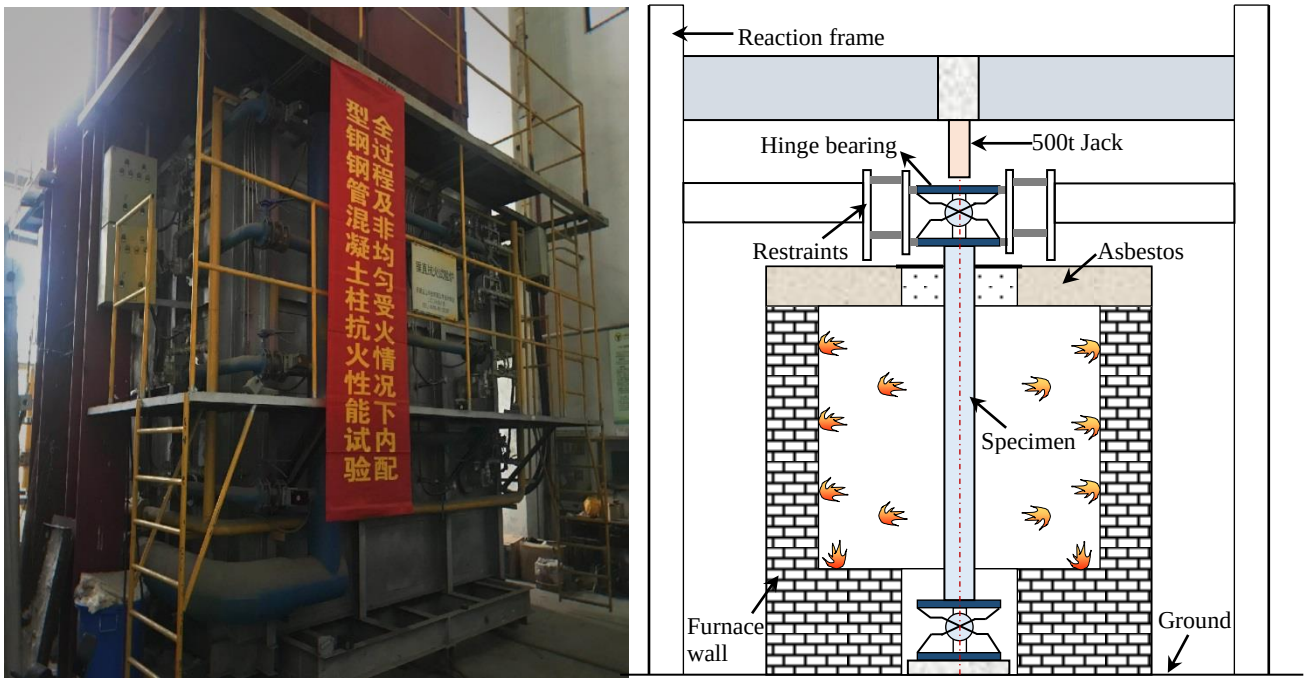

(a) Photo of furnace (b) Schematic diagram of test setup

Fig.3. Fire test setup

(a) Bottom end (b) Top end

Fig.4. Test boundary conditions

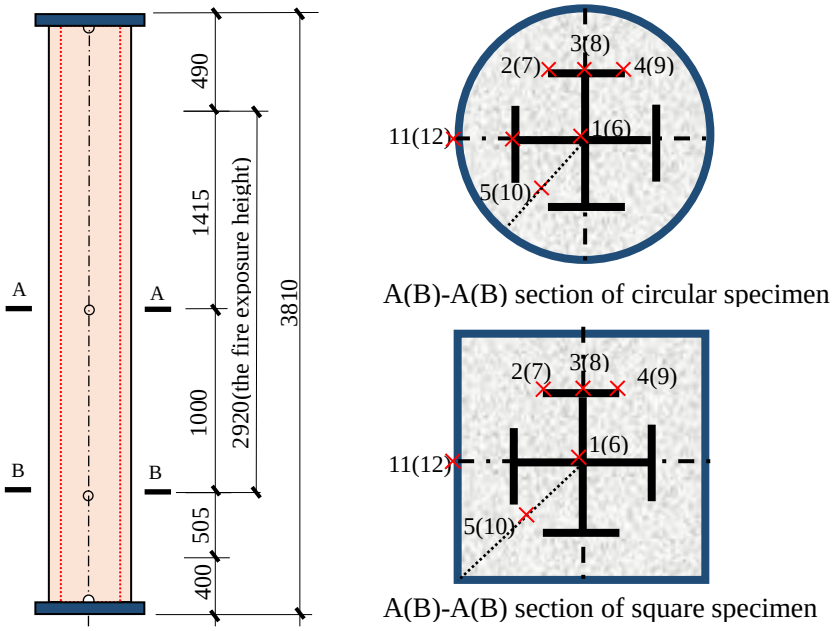

Fig.5. Positions of thermocouples (unit in mm)

Fig.6. Failure modes of the specimens

(a) CSU-P50-40 (b) SSU-P50-40 (c) The concrete mortar (d) The surface of steel tube

Fig.7. Local details of the specimens

(a) Circular steel tube after being cut open

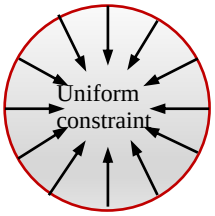

(b) Confinement effect of circular tube

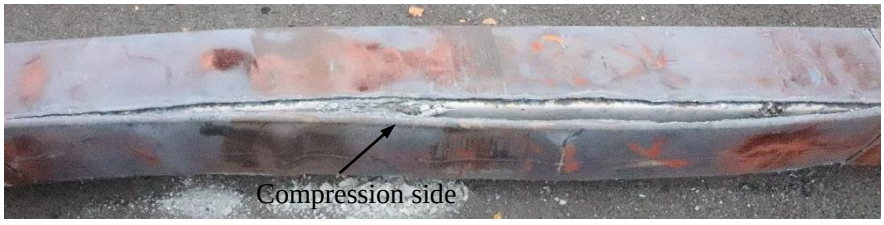

(c) Square steel tube after being cut open

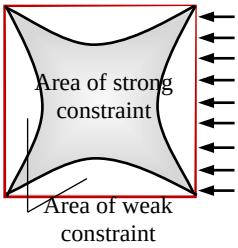

(d) Confinement effect of square tube

Fig.8. The confinement effect of the specimen section

(a) Overall (b) Local

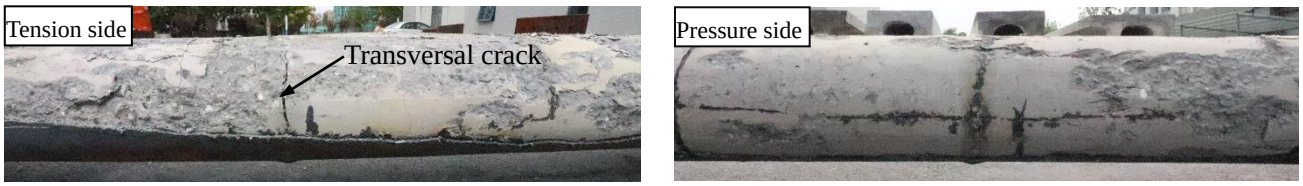

(c) Concrete at tension side (d) Concrete at compression side

Fig.9. Concrete failure mode of CSU-Z-40

(a) Overall (b) Local

(c) Concrete at tension side (d) Concrete at pressure side

Fig.10. Concrete failure mode of SSU-Z-40

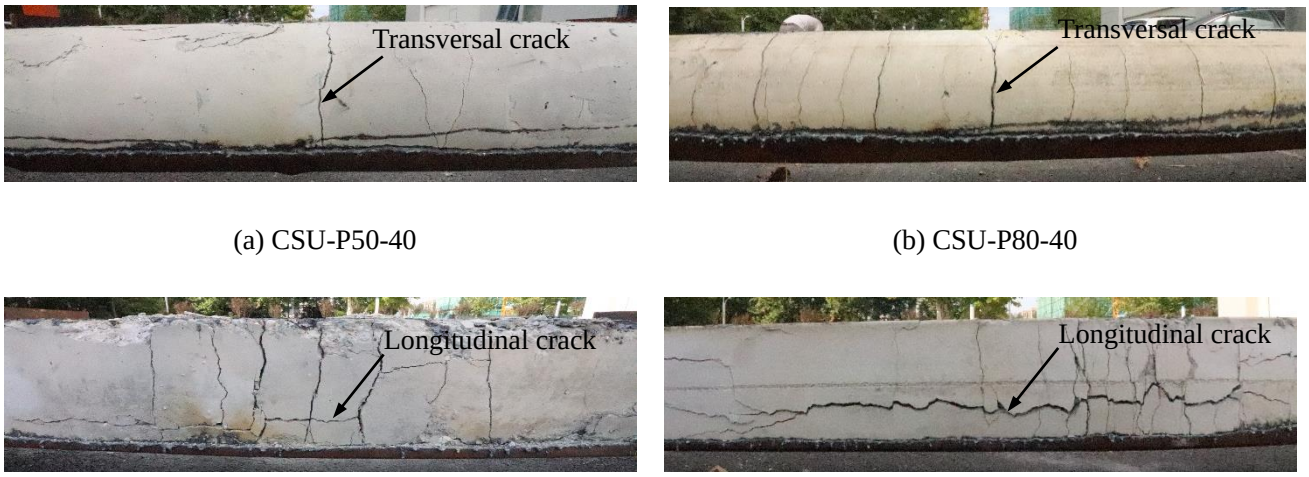

(a) CSU-P50-40 (b) CSU-P80-40

(c) SSU-P50-40 (d) SSU-P80-40

Fig.11. Concrete failure mode of eccentric compression specimens at tension side

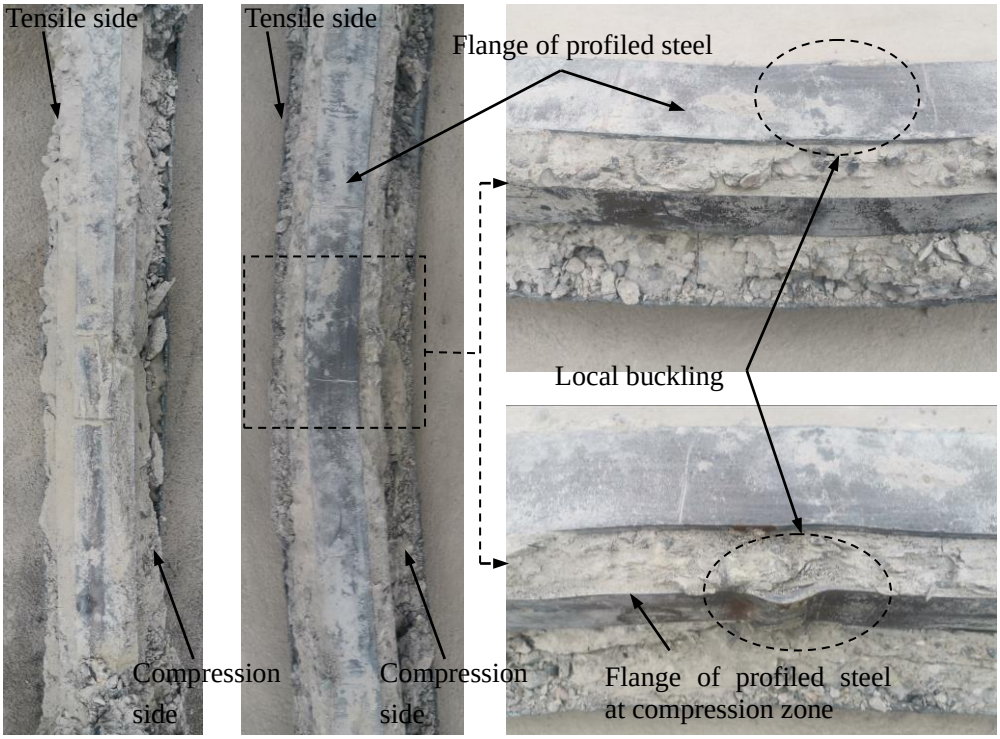

(a) CSU-P80-40 (b) SSU-P80-40

Fig.12. Failure modes of profiled steel

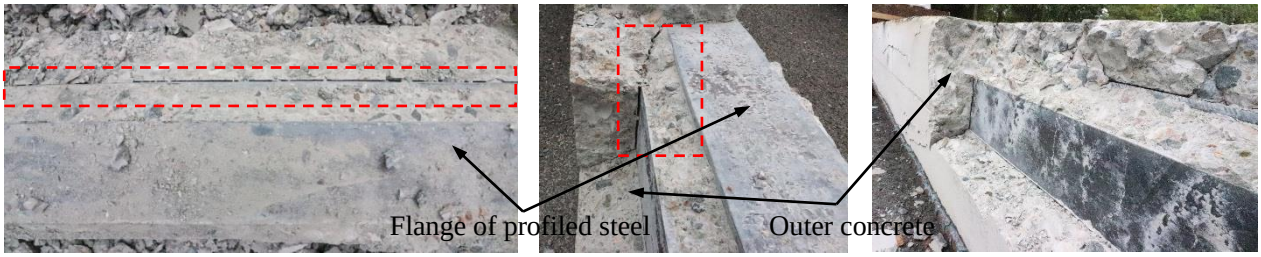

(a) Inner state

(b) External state

Fig.13. Views of interface between outer concrete and profiled (SSU-P80-40)

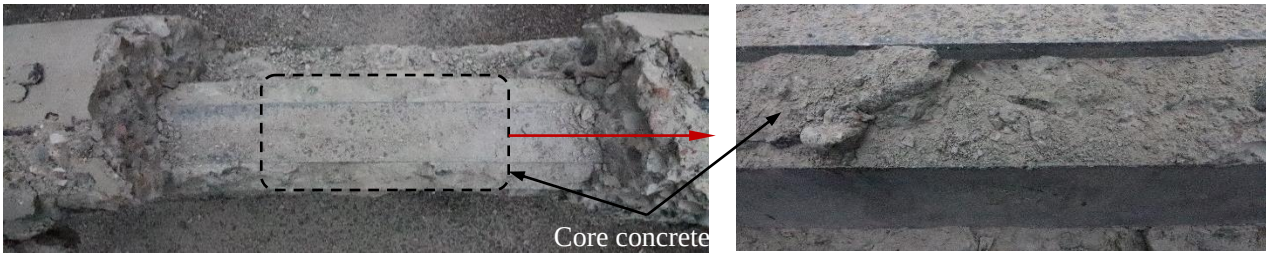

Fig.14. Failure modes between profiled steel and core concrete

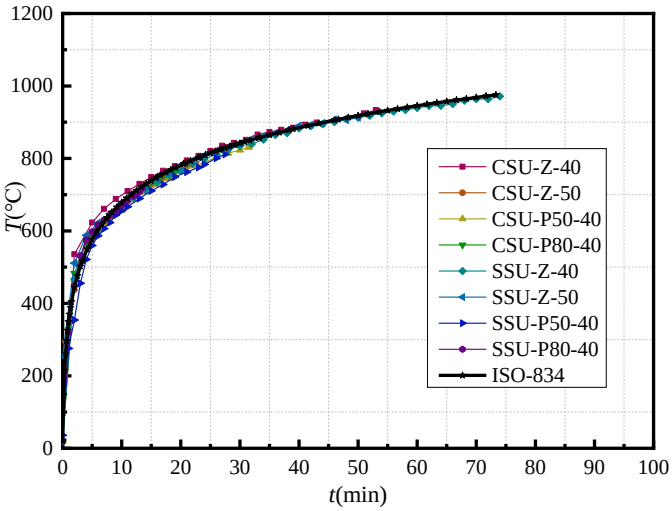

Fig.15. Measured furnace temperature (*T*) versus time (*t*) relationships

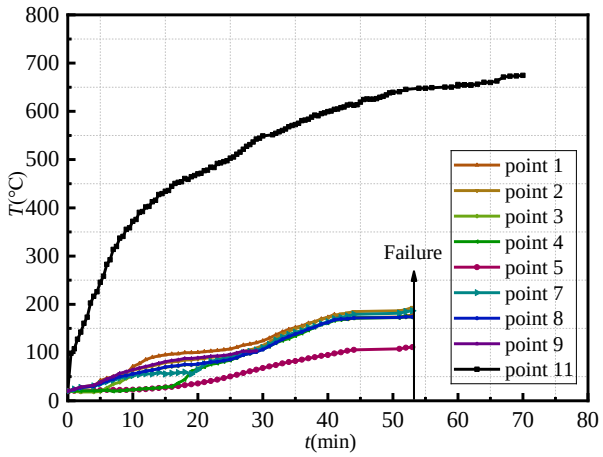

(a) CSU-Z-40

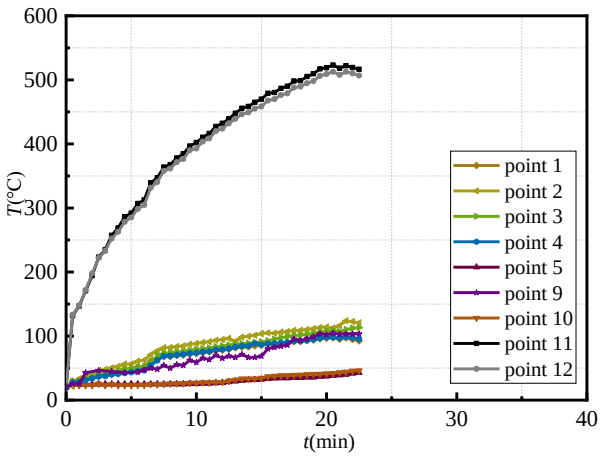

(b) CSU-Z-50

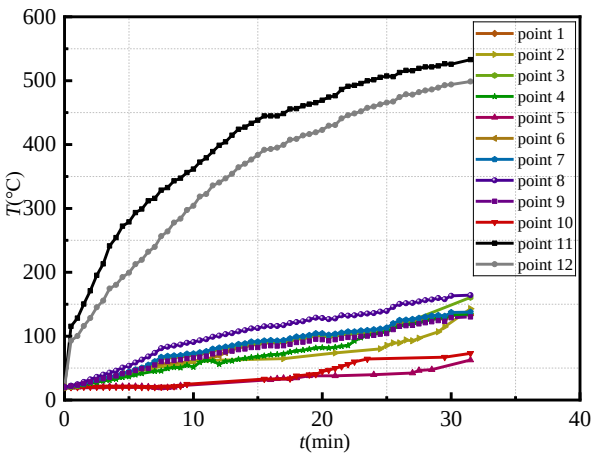

(c) CSU-P50-40

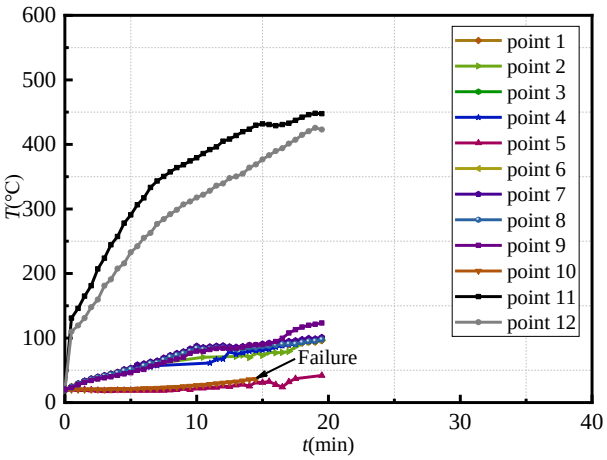

(d) CSU-P80-40

Fig.16. Measured temperature of steel reinforced concrete filled circular steel tubular columns

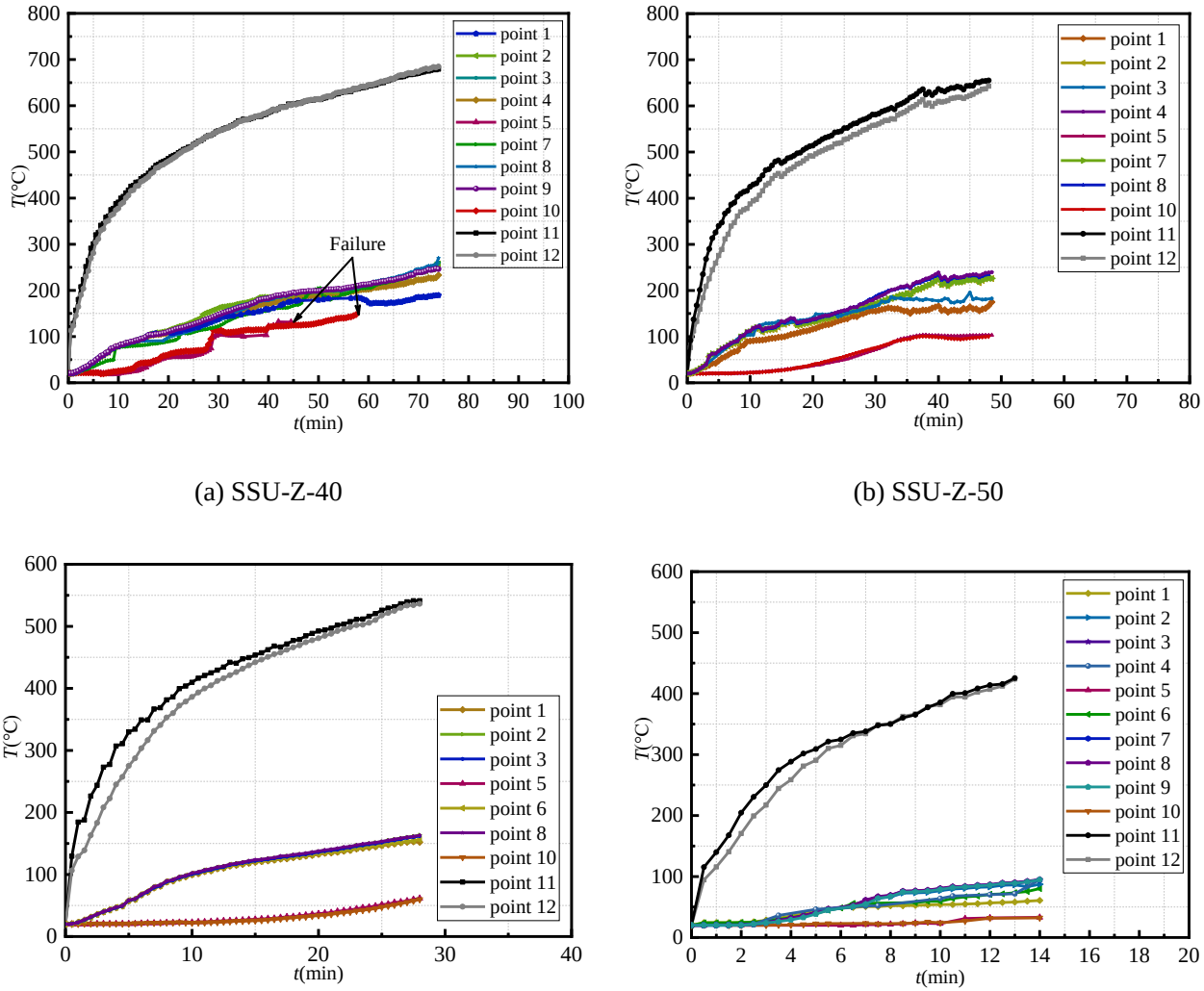

(a) SSU-Z-40

(b) SSU-Z-50

(c) SSU-P50-40

(d) SSU-P80-40

Fig.17. Measured temperature of steel reinforced concrete filled square steel tubular columns

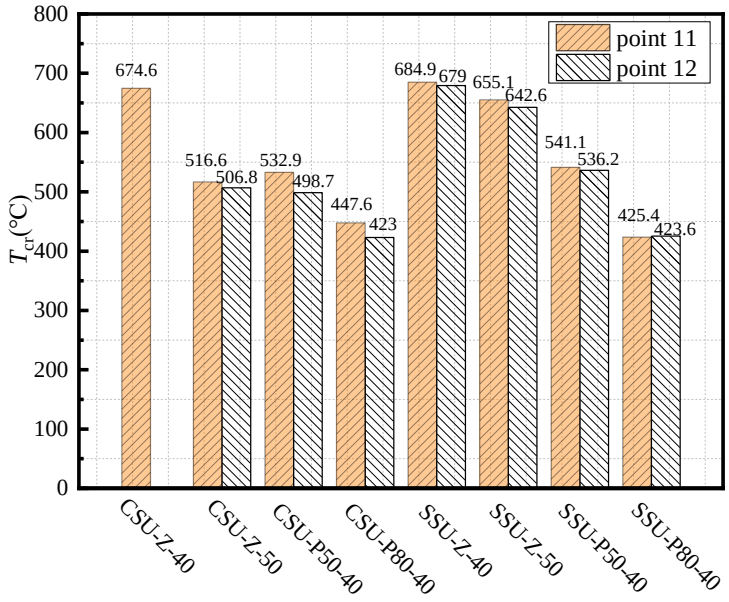

Fig.18. Measured temperature on surface of steel tube

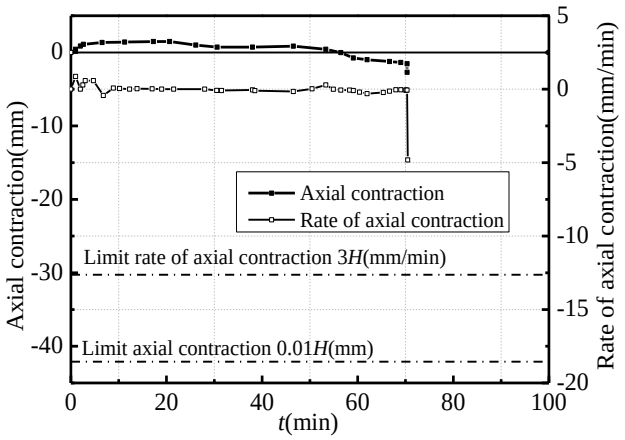

(a) CSU-Z-40

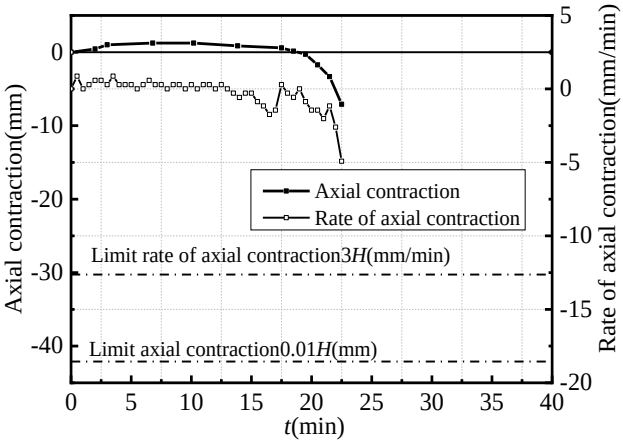

(b) CSU-Z-50

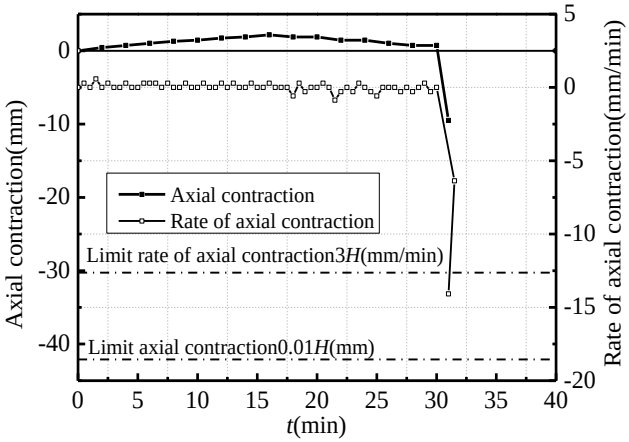

(C) CSU-P50-40

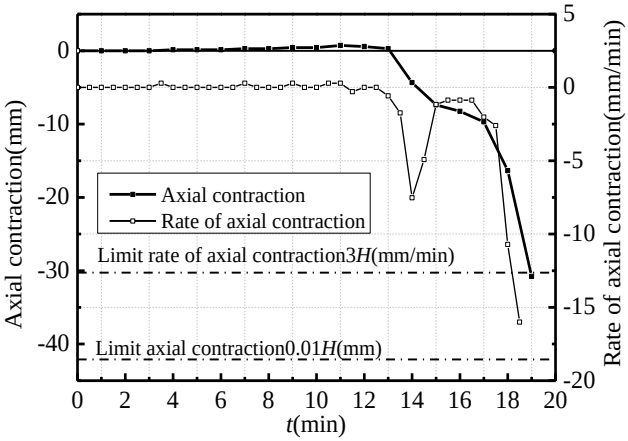

(d) CSU-P80-50

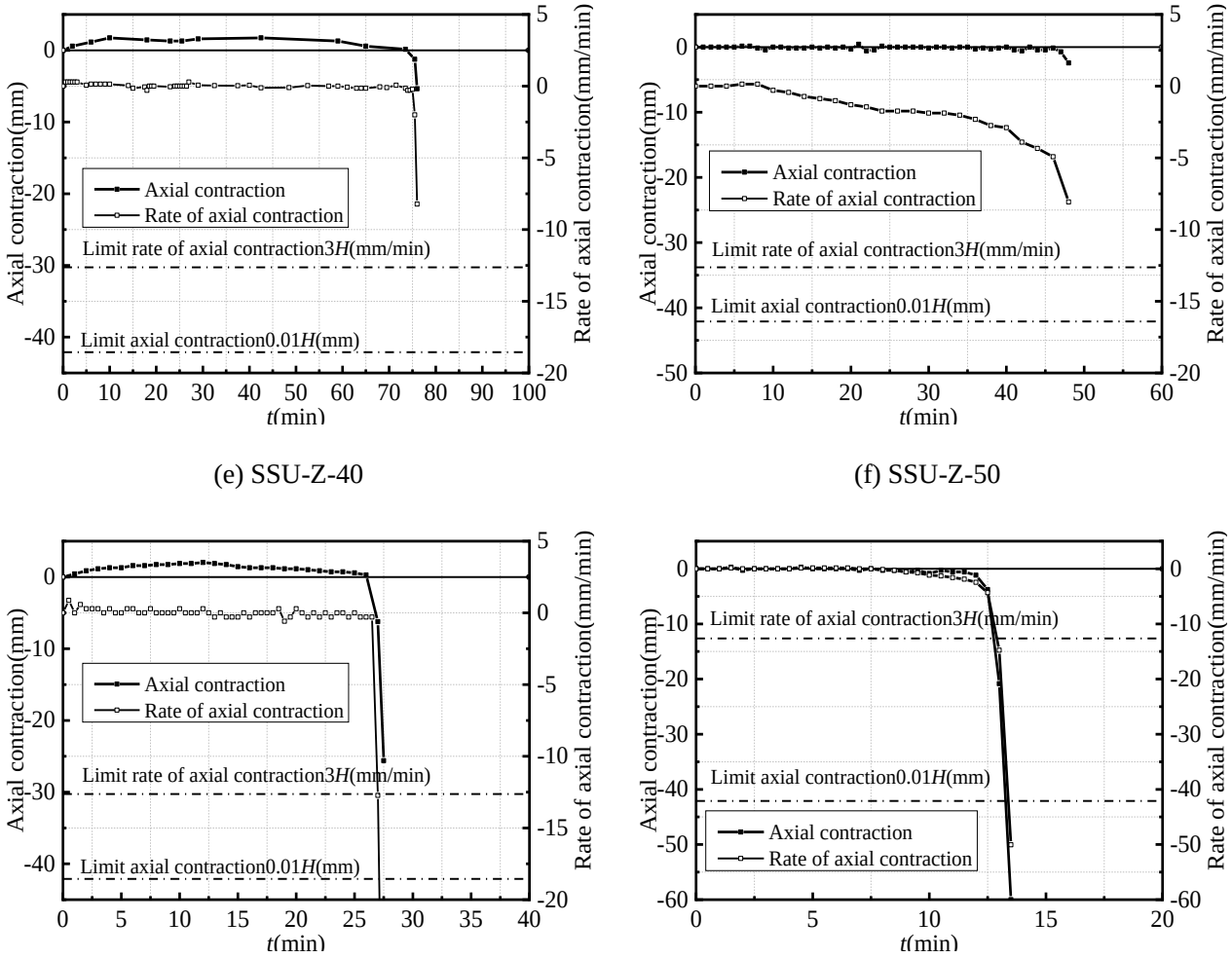

(e) SSU-Z-40

(f) SSU-Z-50

(g) SSU-P50-40

(h) SSU-P80-40

Fig.19. Axial deformation versus time relationship

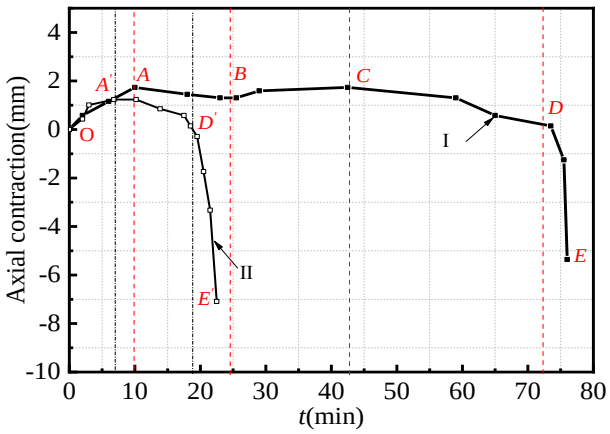

Fig.20. Typical axial deformation versus time relationship

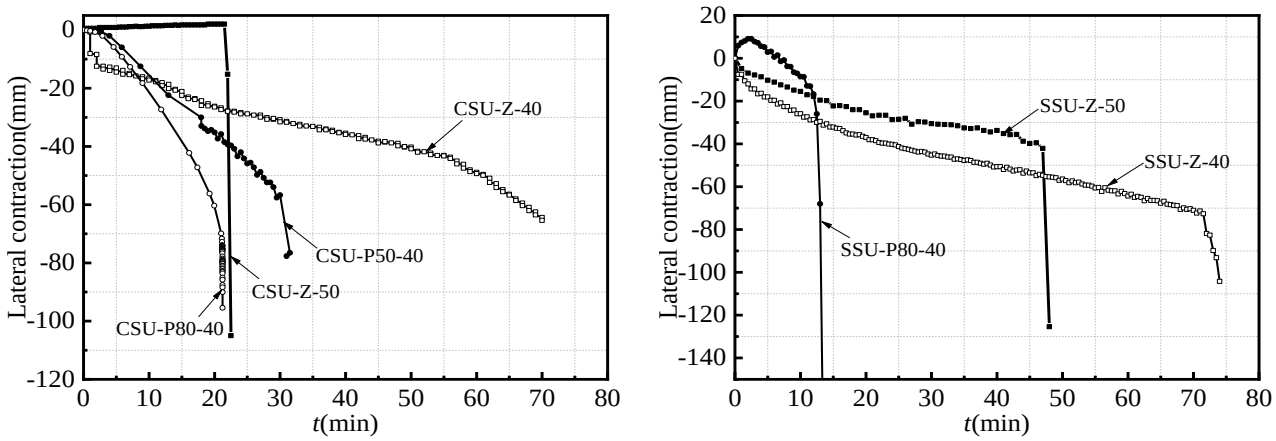

(a) Circular SRCFST columns (b) Square SRCFST columns

Fig.21. Lateral deformation versus time relationship

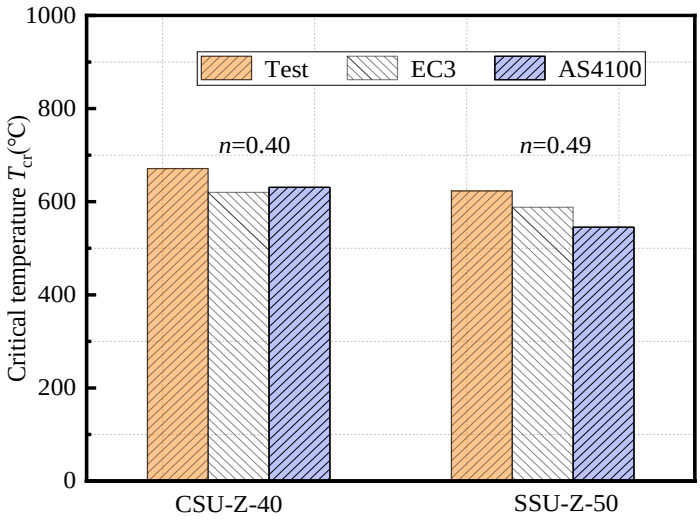

Fig.22. Comparisons of critical temperatures under different load ratio

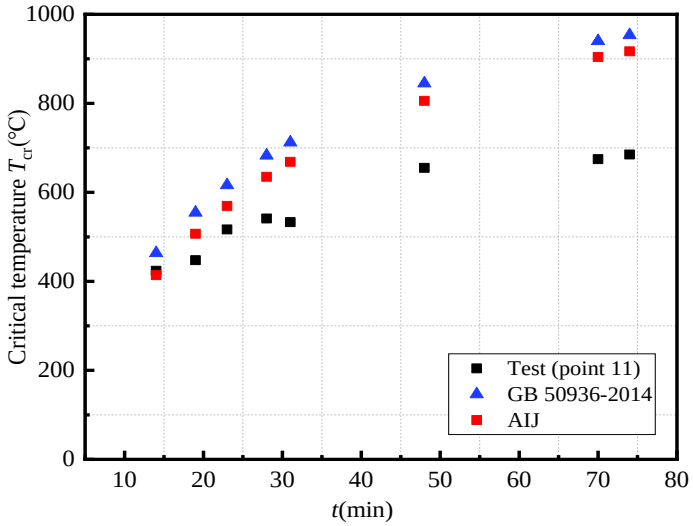

Fig.23. Comparisons of critical temperature on steel tube between simplified methods and tests

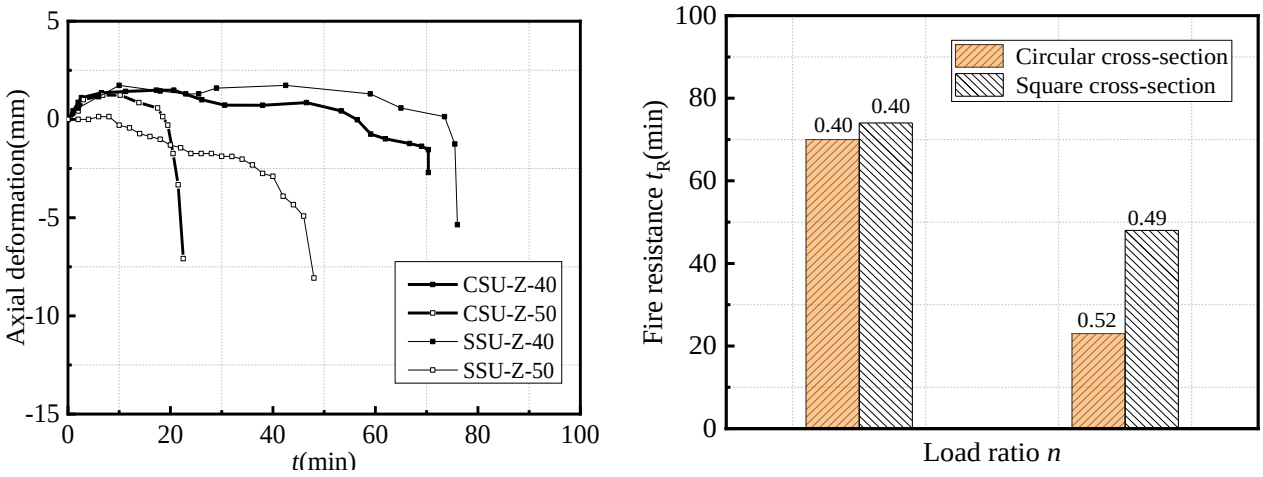

(a) Axial deformation versus time relationship

(b) Comparison of fire resistance

Fig.24. Influence of load ratio on fire resistance

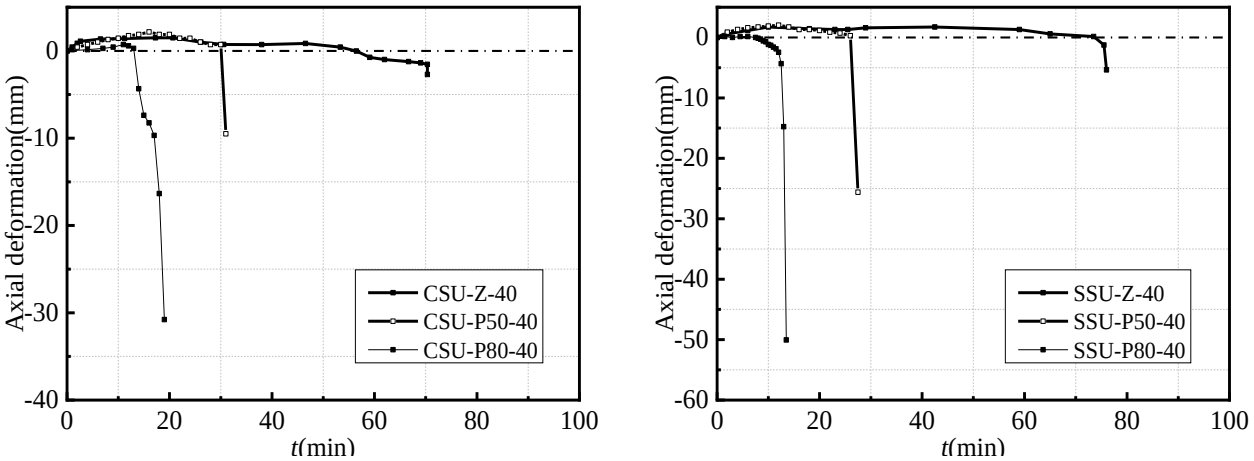

(a) Axial deformation of circular cross-section (b) Axial deformation of square cross-section

Fig.25. Influence of eccentricity on axial deformation

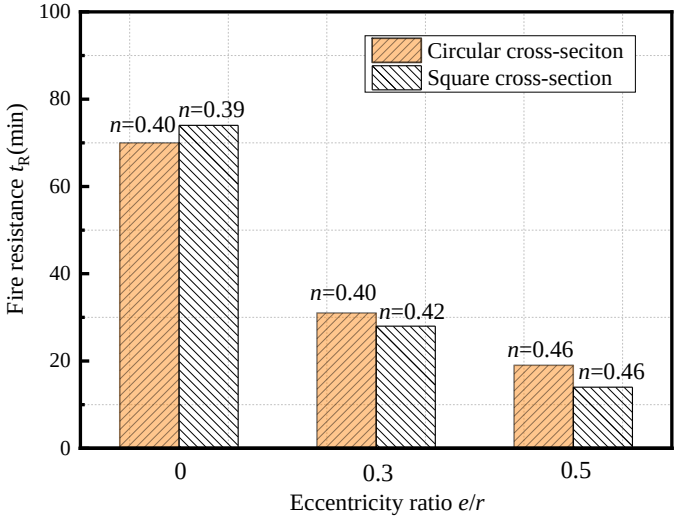

Fig.26. Influence of eccentricity on fire resistance

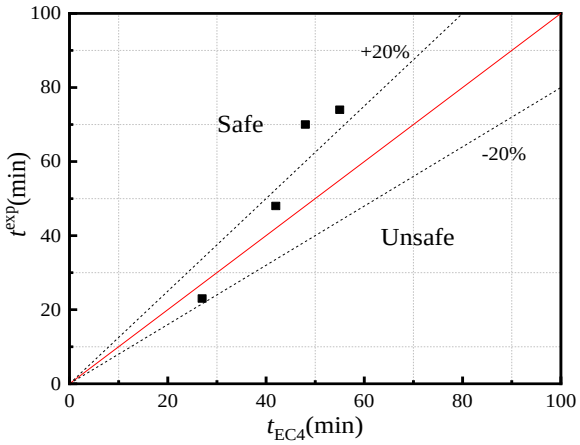

(a) Fire resistance predicted by EN 1994-1-2

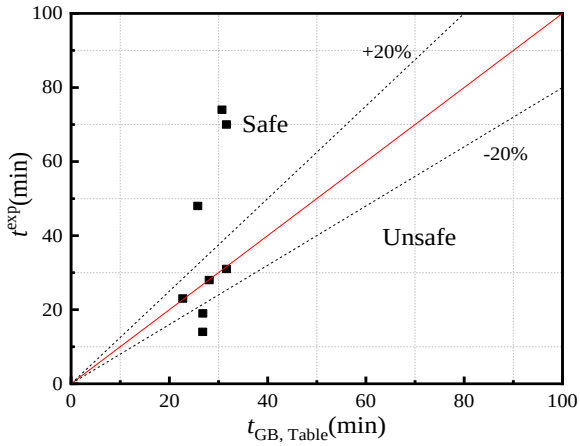

(b) Fire resistance predicted by tabulated data in GB 50936-2014

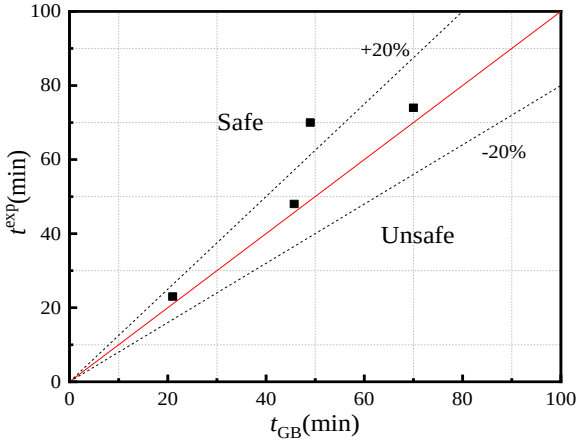

(c) Fire resistance predicted by GB 50936-2014

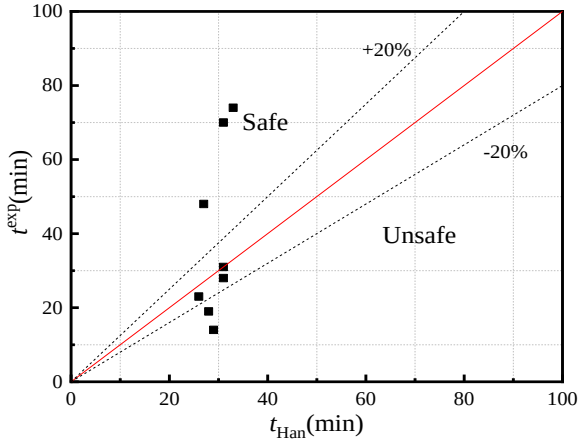

(b) Fire resistance predicted by Han

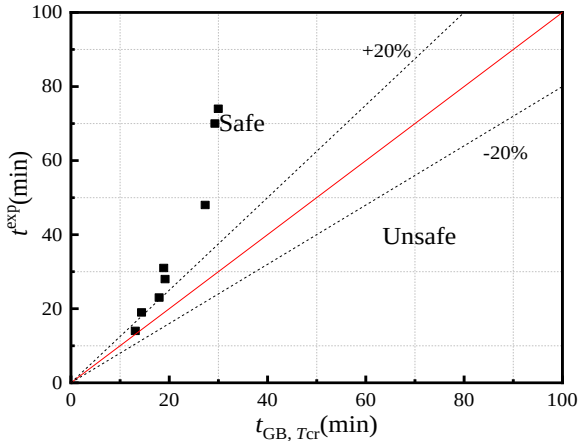

(d) Fire resistance predicted by critical temperature in GB 50936-2014

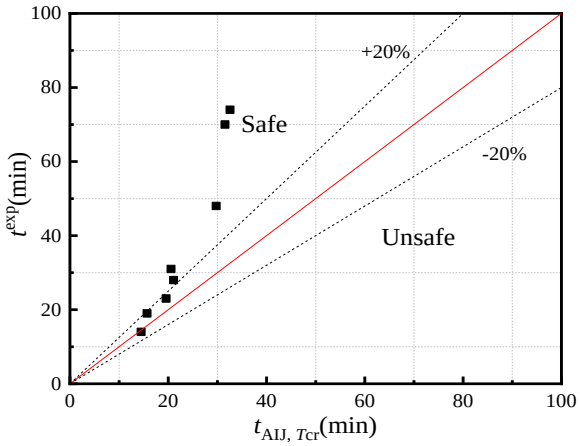

(e) Fire resistance predicted by critical temperature in AIJ

Fig.27. Comparison between test results of SRCFST specimens and predicted fire resistance

Captions for Tables

Table 1 Summary of specimen information

Table 2 Material properties of steel

Table 3 Details about apparent characteristics of steel tube for fire resistance test

Table 4 Predicted fire resistance for SRCFST specimens

Captions for Figures

Figure 1 Typical cross-sections of SRCFST members.

Figure 2 Details of the specimens (units in mm)

Figure 3 Fire test setup

Figure 4 Test boundary conditions

Figure 5 Position of thermocouples

Figure 6 Failure modes of the specimens

Figure 7 Local details of the specimens

Figure 8 The confinement effect of the specimen section

Figure 9 Concrete failure mode of CSU-Z-40

Figure 10 Concrete failure mode of SSU-Z-40

Figure 11 Concrete failure mode of eccentric compression specimens at tension side

Figure 12 Failure modes of profiled steel

Figure 13 Views of interface between outer concrete and profiled (SSU-P80-40)

Figure 14 Failure modes between profiled steel and core concrete